LUND UNIVERSITY

Master of Science
Thesis
VT2023

Polymer gel dosimetry with MRI-readout for 3D dose verification - detector characteristics and clinical applications

Thi Guldhill

Supervisors

Sofie Ceberg, Anneli Edvardsson, Crister Ceberg, Christian Jamtheim Gustafsson, Patrik Brynolfsson, and Sven Bäck

Medical Radiation Physics, Lund
Faculty of Science
Lund University
www.msf.lu.se

Populärvetenskaplig sammanfattning

Att säkerställa strålning på rätt plats i tre dimensioner

Strålbehandling är en viktig behandling av cancer och det är avgörande att ge de föreskrivna stråldoserna exakt på rätt plats för att lyckas. Innan en patient behandlas verifieras strålbehandlingen genom kontrollmätningar. Dessa kontrollmätningar utförs med små detektorer som är placerade i ett fantom. Dessa mäter dosen endast i de punkter där de placeras. Stråldosen som ligger mellan dessa punkten har man dock liten kännedom till.

Geldosimetern är en detektor med hög upplösning och kan mäta dosfördelningar i en hel volym i tre dimensioner (3D), en unik och önskvärd egenskap. En sådan detektor är speciellt användbar för att kunna säkra att nya behandlingsmetoder med avancerade dosfördelningar kan levereras på ett korrekt sätt till en patient.

Geldosimetern består till mestadels av vatten och gelatin samt kemikalier som har förmåga att polymeriseras när den exponeras för strålning. Denna förändring av gelen kan detekteras med en magnetresonanskamera.

En typ av geldosimeter som undersöktes i detta arbete är N-Isopropylacrylamide (NIPAM) geldosimeter. I denna studie utvärderades dosimeters respons till strålning av olika strålslag. Som en klinisk applikation användes NIPAM-baserad geldosimeter för att verifiera stråldosen från en behandling av flera hjärnmetastaser för att visa dosimeterns tillämpning för 3D-mätningar. Gelen bestrålades med olika typer av strålning och kliniskt relevanta doser.

NIPAM geldosimeter uppvisade en bra uppskattad linjär respons för olika strålningstyper och dessutom hade geldetektorn en hög upplösning. Geldosimeter visade en oberoende respons för varierade energier och dosrater. En lägre signal visades vid protonstrålningsmätning vilket kräver korrigeringar för framtida mätningar. Beträffande den kliniska applikationen visade geldosimeters uppmätta 3D dos en god överensstämmelse med den planerade hjärnmetastas-behandlingen.

I denna studie har ett arbetsflöde för geldosimetri utvecklat, inklusive ny laboratorieutrustning, nya utläsningsmetoder samt nytt analysverktyg. Resultaten av denna studie har förbättrat förståelsen av NIPAM geldosimeters egenskaper och visar på kliniska tillämpningar för noggrann bedömning av 3D-dosfördelningar.

Abstract

Background & Purpose: Radiation therapy is an essential treatment for cancer patients with the ultimate goal to deliver radiation doses to the tumour with precision while minimizing exposure to surrounding healthy tissues. Treatment verification is crucial to ensure the accuracy of radiation delivery, for instance by measuring the radiation dose distribution. Among various dosimetry techniques, gel dosimetry has emerged as a promising method due to its ability to measure 3D dose distribution with high spatial resolution. The overall aim of this thesis is to assess the applicability of normoxic polymer NIPAM gel dosimeters with MRI readout in clinical practice. Specific goals include 1) Investigating and optimising the gel dosimetry workflow containing new laboratory equipment, new MRI sequences during readout and novel software for analysis 2) Evaluating different characteristics of the dosimeter for various types of radiation qualities and 3) Using the dosimeters for a 3D dose verification of a clinically novel radiotherapy treatment techniques.

Material & Method: The NIPAM gel dosimeter was produced by dissolving gelatin in deionized water. N'-methylenebisacrylamide (BIS) and n-isopropyl acrylamide (NIPAM) together with antioxidant tetrakis (hydroxymethyl) phosphonium chloride (THPC) were added. The gel was then exposed to different radiation qualities (220 kV photon, 6 and 10 MV photon, and 120 MeV proton beams) with varying setups to investigate the dose-response for clinically relevant dose range, the resolution, the interbatch & intrabatch variation and the dose rate & energy dependency. Readout was done using a clinical MRI (3 T). In the application of 3D measurement, the NIPAM gel dosimeter was used to verify a multiple brain metastases stereotactic HyperArc photon treatment. The dose distribution acquired from the gel measurement was compared with the dose distribution from the treatment planning system using different gamma criteria.

Result: NIPAM-gel dosimeter exhibited an approximately linear dose response for various types of radiation, including 220 kV photons, 6 and 10 MV photons, and 120 MeV proton at the plateau region. The gel dosimeter demonstrated a high spatial resolution. Intrabatch variation showed good consistency with a standard deviation within 1%. The interbatch deviation was found with a maximum of 7% at 26 Gy. No dose rate dependency was found for dose rates of 600 MU/min and 300 MU/min within the 0-15 Gy dose range. Similarly, no energy dependency was observed for 6 MV and 10 MV within the same dose range. When measuring the depth dose curve of the proton beam, the dosimeter exhibited a quenching effect of 40% to 45% in the Bragg peak due to higher linear energy transfer.

The result from verification of multiple brain metastases stereotactic HyperArc photon treatment showed pass rates of 99.94% and 99.87% (5%/5mm); 96.46% and 91.91% (3%/3mm) and 92.21% and 83.44% (3%/2mm) for 50% of dose and 90% of dose (global gamma), respectively when compared to treatment planning system.

Conclusion: The work within this study has developed and improved a workflow for gel dosimetry, incorporating the use of new laboratory equipment, new MRI sequences during readout, and novel software for data analysis. Further, the results of

this study enhance the understanding of NIPAM-gel dosimeter characteristics and showed potential use for clinical applications in accurately assessing 3D dose distribution.

Keywords: gel dosimetry, polymer gel, NIPAM, MRI, proton, HyperArc, QA.

List of Acronyms

Below is the list of acronyms that have been used throughout this thesis listed in alphabetical order:

BIS	N,N'-methylene-bis-acrylamide
CT	Computed tomography
DD	Dose deviation
DTA	Distance to agreement
GTV	Gross tumor volume
IMRT	Intensity-modulated radiation therapy
LET	Linear Energy Transfer
MRI	Magnetic resonance imaging
MU	Monitor unit
NIPAM	N-Isopropylacrylamide
PT	Proton therapy
PTV	Planning target volume
QA	Quality assurance
R_2	Transversal relaxation rate
SRS	Stereotactic radiosurgery
TE	Echo time
THPC	Tetrakis(hydroxymethyl)phosphonium
TPS	Treatment Planning System
T_2	Transversal relaxation time
TR	Repetition time
VMAT	Volumetric modulated arc therapy

Contents

1
Introduction

A rise in life expectancy has made cancer one of the leading causes of death [1]. Cancer treatment has become an important aspect of modern health care. Radiotherapy has become an essential treatment for cancer and contributes to approximately 40% of curative treatments [2]. The ultimate goal of radiotherapy is to deliver high doses to tumours while sparing the surrounding normal tissues in order to achieve both therapeutic effects and minimal side effects.

For the past decades, the technique for radiotherapy has advanced remarkably. As sophisticated treatment techniques, such as intensity-modulated radiation therapy (IMRT), Volumetric modulated arc therapy (VMAT), stereotactic radiosurgery (SRS), and pencil beam scanning proton therapy (PT) have been established, the dose distribution for radiation therapy has become both more conformal and more complex.

As part of the quality assurance protocols, procedures are established to ensure that the radiotherapy machine delivers the planned dose with accuracy and safety within the established criteria. Treatment verification is a vital link in external beam radiation therapy. For patient-specific QA and verification of new treatment techniques, treatment plans are delivered on a phantom with dosimeters inside to calculate the specific dose distribution and compared with dose distribution from the treatment planning system. The dosimeters inside the phantom are normally ionization chambers, diodes or films. They are often arranged in arrays and/or in orthogonal planes in the phantom. Figure 1.1 shows a common detector established in patient-specific QA-link, the Delta^4 phantom+ (Scandidos). The phantom consists of 1069 p-doped Silicon diodes. In the central area (6x6 cm), the diodes are placed 5 mm apart and 10 mm on the outside [3]. The Delta^4 is not susceptible to variation in handling, having direct reading and convenience of use making it a good fit for daily clinical routine [3].

In order to verify a treatment plan, both dosimetric and spatial information needs to be validated. However, inside the mentioned phantom geometry (e.g. Delta^4), diodes or chambers are placed at a distance apart. These diodes/chambers integrate dose over a volume and software reconstructs 3D dose distribution from a limited number of measurement points. Consequently, the need for high-resolution dosimetry is highly relevant as radiotherapy dose distributions are more complex.

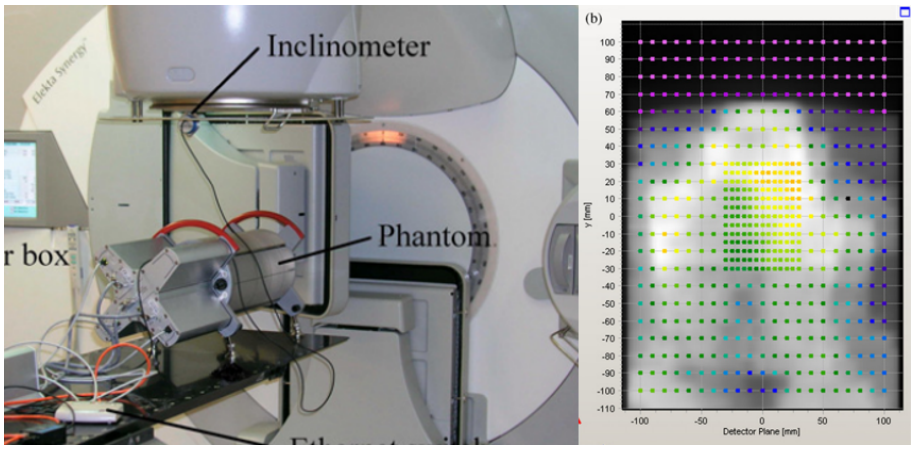

Figure 1.1: The Delta^4 phantom+ (Scandidos) positioned on a treatment couch and its typical output with the planned dose distribution in greyscale and the measured dose in colour over the main detector board. Figures are from Bedford et al. [3].

When compared to other commonly used dosimetry systems such as film, ionization chambers, and thermoluminescent dosimeters, gel dosimeters exhibit favourable characteristics in many perspectives such as radiologically soft-tissue equivalent, high spatial resolution, high sensitivity and directional independence [4] [5]. Previous studies have shown that polymer gel dosimetry can be integrated into QA-link and used to evaluate new techniques in the clinic [6] [7]. Gel dosimetry has the potential to be a valuable tool as an independent 3D detector system for treatment benchmarking, particularly when introducing new radiotherapy treatment techniques.

2
Aims

The overall aim of this thesis was to investigate N-isopropyl acrylamide (NIPAM) gel dosimeters, utilizing magnetic resonance imaging (MRI) readout method, as an independent detector tool for assessing dose distribution in 3D. To achieve this overall aim, the following goals were established:

- To investigate and optimize the gel dosimetry workflow including new laboratory equipment, new MRI sequences during readout and novel software for analysis.
- To determine the fundamental characteristics of NIPAM-gel dosimeter with MRI-readout including linearity of dose-response for different radiation qualities (photon and proton) in clinically relevant dose range, inter batch & intrabatch variation, small field, different dose rates (300 MU/min and 600 MU/min) & different energies (6 MV and 10 MV).
- To demonstrate a clinical application with verification of a clinical multiple metastases HyperArc SRS photon treatment delivery using NIPAM gel dosimeter.

3

Theory

3.1 Radiotherapy techniques

3.1.1 Advance photon radiation

Volumetric modulated arc therapy (VMAT) was first introduced in 2007 as a novel radiation technique that enabled the simultaneous control of gantry rotation speed, multi collimator leaf movement to adjust treatment aperture shape and dose rate [8]. Several VMAT systems have been developed and marketed under different names such as RapidArc by Varian, SmartArc by Phillips and Elekta VMAT by Elekta. Compared to conventional radiotherapy techniques, VMAT allows for highly conformal dose distributions that result in better coverage of the target volume and minimize dose to normal tissues. Compared to conventional static field intensity-modulated radiotherapy (IMRT), treatment delivery time in VMAT is shorter [8].
In comparison to conventional radiotherapy, stereotactic radiotherapy, a non-invasive ablative therapy, delivers a higher dose to the targeted area in fewer fractions [9]. Given the administration of a higher dose per fraction, the margin of error in SRS is smaller compared to conventional radiotherapy [10].
HyperArc (Variant Medical System, Milpitas, CA) VMAT SRS is a novel SRS technique. In HyperArc, the collimator angle and field size together with the treatment couch angle are optimized using one single isocenter. Compared to conventional VMAT, optimization of the procedure with HyperArc treatment plan is faster and the maximum dose is higher [11] [12]. Furthermore, HyperArc employs high-definition multi-collimator leaves to enable SRS dose delivery for small targets, by that reducing irradiation to organs at risk and normal tissue [12].

3.1.2 Proton therapy

Proton beams have two important regions, the proximal (also referred to as the plateau region) and the Bragg peak (also referred to as the maximal). The proximal region is characterized by a relatively constant energy deposition before the Bragg peak, while the Bragg peak is where protons deposit the maximum amount of energy. A distal fall-off region can be seen after the Bragg peak with the rapid decline in energy deposition after the peak region. A comparison of the depth dose profile of photons and protons and Spread Out Bragg Peak (SOBP) are shown in Figure 3.1a. After the buildup region, linear energy transfer (LET) along depth for photon is considered constant while in proton LET during the track varies significantly. The depth dose curve of proton and its linear energy transfer is illustrated in Figure

3.1b. The SOBP is created by combining multiple Bragg peaks of different energies to create a plateau of energy deposition in order to cover tumours of irregular shapes. In pencil beam scanning, a proton beam is broken down into small beams, hence the name pencil beams. By varying the position of the proton beam, a dose plan can be delivered with a desirable precise pattern [13].
Skandion Clinic located in Uppsala, Sweden is a cancer treatment centre which is equipped with a state-of-the-art pencil beam scanning system for proton therapy. The beam scans across the tumour in a series of small spots, with the energy and intensity of each spot adjusted based on the shape and depth of the tumour, as well as the density of the tissue it is passing through which allows for precise targeting of the tumour and sparing of healthy tissue. The delivery energy can be in a range from 55 MeV to 230 MeV (2.82 cm to 33.80 cm in terms of range in water).
The linear energy transfer quantity is defined as follows by the International Commission on Radiological Units (1962): The LET of charged particles in a medium is the quotient of dE/dl, where dE is the average energy locally imparted to the medium by a charged particle of specified energy in traversing a distance dl:

$$LET = \frac{dE}{dl} \tag{3.1}$$

At the microscopic level, the energy per unit length of the track varies over a wide range, and therefore LET is an average quantity. LET usually has the unit keV/μm. X-rays and γ rays are considered low LET radiations which are sparsely ionizing, while high energetic protons, neutrons and heavily charged particles are high LET radiations which are densely ionizing [14].

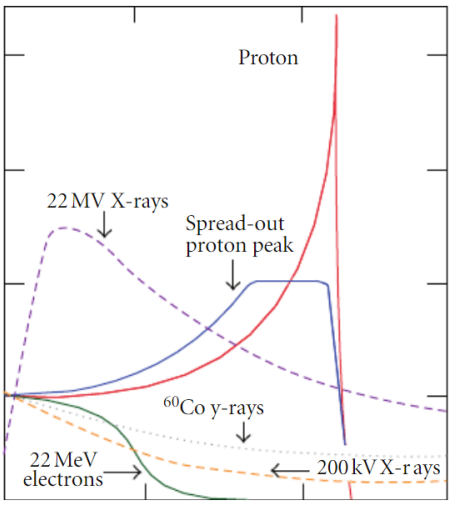

(a) Depth dose curve of a proton (Bragg peak) and Spread out proton peak (Spread-Out Bragg Peak), in comparison with photons (MV and kV) and electron, figure is from Cianchetti et al. [15].

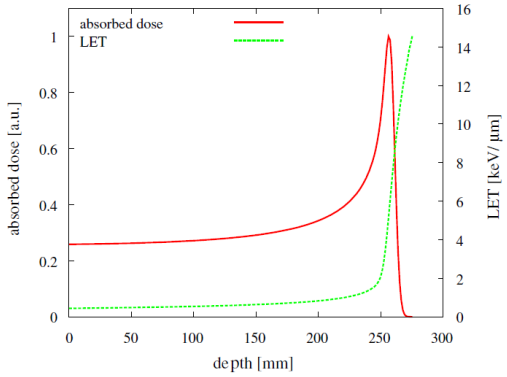

(b) Depth dose curve in water and corresponding LET. The figure is from Frese et al. [16].

Figure 3.1: Depth dose curve of different radiations and depth–dose curve of a monoenergetic proton and relationship to linear energy transfer (LET).

3.2 The fundamental of polymer gel dosimetry

A gel dosimeter commonly contains water, a gelling agent and an agent which responds to irradiation. The gel dosimeters which are commercially available are Fricke gel dosimeters, polymer gel dosimeters and two novel types of gel dosimeters (micelle gel dosimeters and genipin gel dosimeters) [17], sorted based on their mechanism. Fricke gel dosimeters exploit the oxidation of ferrous sulfate into ferric ions. Polymer gel dosimeters are those based on polymerization reactions induced by the radicals formed during the radiolysis of water. Micelle gel dosimeter consists of leuco-dye molecules that react with free radicals generated by water radiolysis and change colour while genipin gel dosimeter consists of genipin, a natural cross-linker which changes colour in response to irradiation [18].
Polymer gel dosimeters (including NIPAM-gel) contain water and gelatin, together with monomers and crosslinkers and antioxidants. Gelatin and water give the dosimeter block structure. Antioxidants maintain the ability of polymerization. Monomer and crosslinker polymerize in response to free radicals triggered by the water radiolysis process, forming networks of polymer chains [5]. The total weight percent, denoted w/w, of the monomer and crosslinker in the system (%T) and the concentration of the crosslinker relative to the total monomer (%C) are directly related to the sensitivity polymer gel dosimeter. An increase in %T and %C crosslinker concentration are likely linked to higher dose sensitivities [17].
For NIPAM polymer gel dosimeter, N,N'-methylenebisacrylamide (BIS) is the crosslinker,

n-isopropyl acrylamide (NIPAM) is the monomer and tetrakis (hydroxymethyl) phosphonium chloride (THPC) is the antioxidant. BIS is an effective crosslinker because it has two vinyl groups which are available for polymerization [17]. Oxygen is found to inhibit radiation-induced polymerization through the formation of peroxides [5]. Oxygen can dissolve in the gel solution during manufacturing process. Therefore, THPC, an aggressive scavenger of oxygen, was commonly used to remove oxygen [17].
The basic chemical reaction of polymer gel after irradiation can be summarized as follows. As irradiation is initiated, free radicals are produced as a result of the radiolysis of water which comprises a large portion of the gel dosimeter. Next, successive propagations and crosslinking reactions occur. The amount of polymer grows and forms the resulting polymer network. From a chemical perspective, it can be briefly concluded that the amount of polymerization is a function of dose [17]. Visually, the amount of resulting polymer network can be detected by the opacity of the gel after irradiation (Figure 3.2).

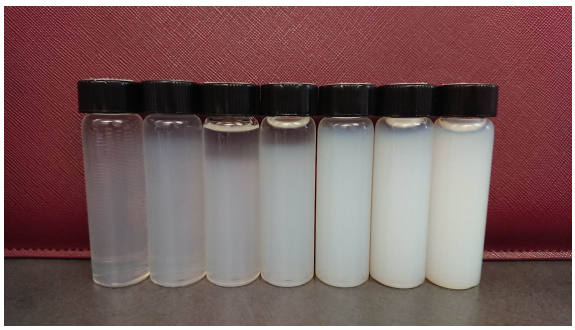

Figure 3.2: Photograph of NIPAM gel dosimeters irradiated with increasing doses (from left to right) to demonstrate the associated visual opacity change. Vials with a higher absorbed dose shows lower opacity.

A compartment model was developed by Ceberg et al. [19] to study the basic dose-response characteristics theoretically (Figure 3.3). Protons in a polymer gel dosimeter can be separated into two groups: one comprises mobile protons (monomers, water) (P1) and one comprises protons associated with the growing polymer (P2) and resulting polymer network (P3).

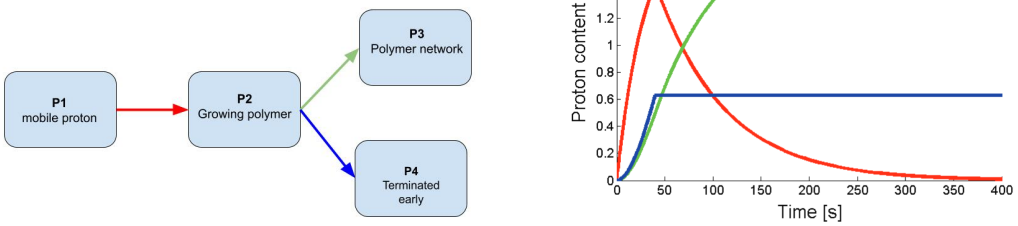

(a) Compartment model of the protons in a polymer gel dosimeter. Upon irradiation, protons from P1 (monomer) are transferred to the growing polymer pool (P2) and further to P3. A part of growing polymerization in P2 can also be terminated early (P4). The figure is adapted from Ceberg et al. [19].

(b) Proton content from different compartments before, during and after irradiation, figure is from Ceberg et al. [19].

Figure 3.3: Compartment model of how proton content in each compartment varies during time.

Before irradiation, at time t = 0, all protons are contained in compartment P1. Protons are transferred from P1 to P2 (red line) when the gel dosimeter is irradiated. Proton from P2 is further transferred to compartments P3 and P4 (green and blue lines). After a sufficient time, all protons originally from compartment P1 have moved onto compartment P3 or the polymerization has been terminated early while compartment P2 is empty [19]. At that time, the gel dosimeter is considered to be stabilized. The compartment model is a rather simplified model but illustrative to understand the complex nature and principle of gel dosimetry system.

3.3 MRI readout for polymer gel dosimeters

The process of obtaining dose distribution of polymer gel dosimetry can be summarized in three steps: First, the radiation-sensitive polymer gel is fabricated and stabilized. Second, the gel dosimeter is irradiated and stabilized. Third, after polymerization, the gel is scanned with an imaging technique.
Magnetic resonance imaging (MRI) can non-destructively measure the magnetization of hydrogen atoms in water molecules in 3D. As irradiation induces a change in the structure of gel through the polymerisation reaction, MRI can be employed as a readout method. Other readout methods utilized for gel dosimetry are optical computer tomography (optical CT), X-ray CT or ultrasound [5].
Local radiation dose and the local concentration of monomer and crosslinker are directly linked to the amount of polymer that forms in the gel dosimeter, given the desirable property of a true 3D dosimeter. This formation of crosslinked polymer

particles induces changes in physical properties. With polymer gel dosimetry utilizing MRI readout, the physical properties transition is the transversal relaxation time or transversal relaxation rate.
Transversal relaxation time, spin-spin relaxation time, also referred as T_2 relaxation is the time by which the transverse components of magnetization (M_{xy}) decay or dephase, first described by Felix Bloch (1946). By the time T_2, M_{xy} has decreased to approximately $37\% \approx \frac{1}{e}$ of its initial value due to the loss of coherence in protons. This loss of coherence is induced by spin-spin interaction from neighbor molecules or magnetic field inhomogeneity [20]. T_2 value is specific for one material. The transversal relaxation rate is the inverse of the transversal relaxation time:

$$R_2 = \frac{1}{T_2} \tag{3.2}$$

The contribution of the relaxation rate can be explained with contributions from the proton in different constituents in gel dosimeter. Lepage et al. [21] proposes an estimation that R_2 is the sum of the respective rates of relaxation weighted by the fraction of free or mobile protons f_{mob}, a growing polyacrylamide network f_{poly} and a gelatin matrix f_{gela}. The rate of relaxation R_2, can be described with Equation 3.3:

$$\frac{1}{T_2} = \frac{f_{mob}}{T_{2,mob}} + \frac{f_{poly}}{T_{2,poly}} + \frac{f_{gela}}{T_{2,gela}} \tag{3.3}$$

As irradiation is initiated, the proportion of different proton pools changes as f_{mob} gradually decreases and at the same time f_{poly} increases while f_{gela} remains unchanged.
As free mobile protons (in water) have relatively long distances and thus have long T_2 time compared to protons in large macromolecules (in polymer). In this case, the mobilizing of f_{mob} to f_{poly} leads to a decrease of T_2 (increasing of R_2).
From the aspect of signal-to-noise (SNR), the multiple spin–echo sequence is preferable [22]. χ^2-minimization algorithm, the most optimal method according to Deene et al. [22], can be used to estimate R_2 by fitting intensities/signals of equidistant consecutive images to a monoexponential decay with equation (Figure 3.4):

$$S = S_0 \cdot e^{-TE \cdot R_2}, \tag{3.4}$$

where S_0 is the signal when the magnetization vector M_{xy} is fully relaxed, echo time (TE) is the interval between the excitation pulse and signal collection.

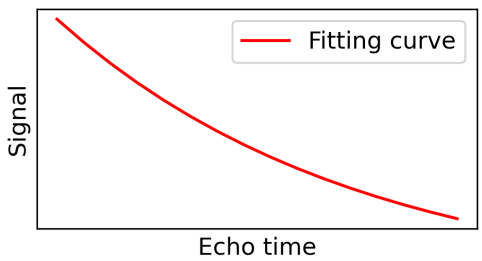

Figure 3.4: Schematically plot of signal against echo time in multi-spin–echo sequence

3.4 Evaluation of dose distributions

When comparing two measurements for example a measured dose distribution to the dose distribution from a treatment planning system, two quantities are typically evaluated: dose deviation (DD) and distance to agreement (DTA). These metrics were introduced by Van Dyk et al. [23] and combined into a single metric known as the Gamma Index (γ), representing the conciliation between the two dose distributions [24].
DD (ΔD_M) is calculated as the absolute difference between the calculated and measured dose values. A high DD value indicates errors in either dose calculation or delivery. On the other hand, DTA or Δd_M, quantifies the spatial accuracy. It is defined as the maximum distance between the calculated and measured dose points, illustrated in Figure 3.5. A smaller DTA value indicates better agreement between the calculated and measured dose distributions [24].
The gamma criteria is usually denoted x%/y mm which refers to the condition for DD and DTA. In specific, for a given point in the dose distribution, if the difference in the measured dose and the calculated dose is less than x% and the distance between the measured and calculated points is less than y mm, the point is considered passed.

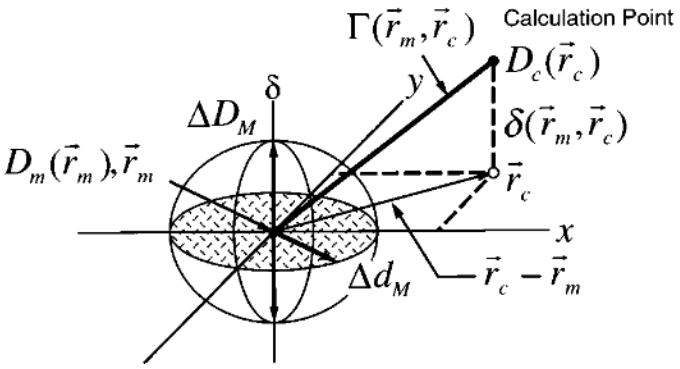

Figure 3.5: Schematically illustration of the γ index concept. The volume of the ellipsoid represents the given acceptance criteria. The calculated dose (reference dose) is $D_c(r_c)$ and the measured dose is $D_m(r_m)$, r denotes the spatial location for measured point r_m and calculated point r_c. Figure is from Low et al. [24].

γ index identifies a quality index at each point in the evaluation plane $r_c - r_m$ for the measurement point r_m:

$$\gamma(r_m) = min\{\Gamma(r_m, r_c)\} \forall \{r_c\}, \tag{3.5}$$

where

$$\Gamma(r_m, r_c) = \sqrt{\frac{r^2(r_m, r_c)}{\Delta d_M^2} + \frac{\delta^2(r_m, r_c)}{\Delta D_M^2}} \tag{3.6}$$

and

$$r(r_m, r_c) = |r_c - r_m|; \qquad \delta(r_m, r_c) = D_c(r_c) - D_m(r_m) \tag{3.7}$$

The pass-fail criteria are defined such that a value of $\gamma(r_m) = 0$ corresponds to an exact match between the measured and calculated doses. The calculation passes if $\gamma(r_m) \leq 1$ and fails if $\gamma(r_m) > 1$ [24].

4
Material & Methods

4.1 Polymer gel fabrication

A gel dosimetry laboratory was further developed by utilizing facilities at Skåne University Hospital (SUS) and Lund University (LU).
The gel manufacturing process is as follows. Gelatin was added to deionized water to swell and stirred with a magnetic stirrer until the gelatin was fully dissolved. The solution was heated up to 45°C. While being stirred continuously, N'-methylenebisacrylamide (BIS) and n-isopropyl acrylamide (NIPAM) were then added and waited until completely dissolved. The solution was then cooled down to 38°C. A solution of antioxidant tetrakis (hydroxymethyl) phosphonium chloride (THPC) was added with 10 mM. The solution was continued to stir for several minutes to ensure complete dissolution. The gel was then poured into glass containers, such as vials or flasks, to solidify. The gel was prepared under normal oxygen levels inside a fume cupboard and the solutions were stirred continuously throughout the mixing procedure. The composition of the gel mixture is described in Table 4.1.
To avoid photopolymerization, the manufacturing process was performed in a relatively dark environment. The concentration of BIS-powder was chosen because the solubility of the crosslinker BIS in the gel was limited to approximately 3% in weight relative to the total weight of the gel mixture [5].
The NIPAM-based gel dosimeter used in the study was relatively toxic. However, if proper chemical safety precautions are followed, the toxicity of the gel dosimeter can be minimized. As a precaution against possible toxicity, the manufacturing process was carried out in a fume cupboard wearing protective clothing (lab coat, goggles, facemask and protective gloves).

Table 4.1: Constituents of NIPAM-gel dosimeter, w/w is the weight relative to the total weight of the gel mixture.

Component	Commercial description	w/w
Gelatin	Gel strength 300 type A, Sigma-Aldrich	5%
BIS	99%, powder, Sigma-Aldrich	3%
NIPAM	97%, powder, Sigma-Aldrich	3%
THPC	80% solution in water, Sigma-Aldrich	10mM
Deionized water	Anthrop Pharmaceutical	89%

4.2 Investigation of characteristics of the NIPAM gel dosimeter

The gel was transferred to small vials (2 cm diameter, 6 cm length) and left to solidify at room temperature for 24 hours. Various investigations, one measurement each, were carried out across ranges of clinically relevant absorbed doses for different radiation qualities. The workflow can be briefly described as follows. First, the gel was manufactured and transferred into containers. Second, the gel dosimeter was irradiated and stabilized. Third, after polymerization, the gel was scanned with MRI readout. Lastly, data analysis was performed.

4.2.1 Dose response photon beam

Gel vials were irradiated in a 220 kV photon beam with an X-ray cabinet irradiator XenX (SARRP, Xstrahl Inc.) (Figure 4.1). A broad focus and 0.5 mm Cu filter were used for all irradiation with a maximum tube potential 220 kV and maximal tube current 13 mA.

Figure 4.1: The Xen-X irradiator

For the linearity test, the gel vials were positioned on two sides of an ionization chamber (diameter 1.0 cm, cylindrical type) on a mounted gantry (Figure 4.2a). An ionization chamber was used to control the linearity of radiation delivered by XenX. Lasers were used to visually align the transverse, sagittal and coronal direction so that the isocenter of the laser was placed in the tip (active region) of the ionization chamber. The position of the couch was defined with a cartesian matrix in XenXs associated program. The coordinates of position were saved to be able to irradiate gel vials at the same source-surface distance (SSD) at 34 cm. The gels were irradiated with different absorbed doses by increasing irradiation time at an estimated dose rate of about 2.5 Gy/min at the isocenter. All the gel vials were irradiated inside the radiation field (10x10 cm^2) with two vials per dose level.
After irradiation, all the vials were placed in a cardboard box again to stabilize and avoid photopolymerization. Two batches with the same gel composition were evaluated.

Conversion factor

As XenX irradiator cabinet was controlled by irradiation time, the dose for each gel vial was converted from irradiation time to absorbed dose by a conversion factor generated from measurements with Gafchromic EBT^3 film (Ashland). The film sheets were cut into pieces of 0.8 x 6.5 cm^2 and placed inside a glass vial filled with water. The film was wrapped inside plastic wrap to ensure no contact with water which might disturb the reading. Handling of the film follows specifications from

the manufacturer. The films were perpendicularly irradiated with 220 kV photon beam with the same setup as gel vials at SSD = 34 cm. The film pieces were then positioned at a 35 cm distance from the source, in the middle of the glass vial because measured ROIs were acquired in the central region of gel vials. Three vials with radiochromic film pieces were irradiated for 60 seconds.
A scanner (Epson, Expression 12000XL) and its associated software were used to scan all the film pieces after irradiation and two background pieces. First, a dry run was performed to stabilize the scanner. Films were scanned with 800 dpi spatial resolution, 8-bit per colour channel and portrait mode. The optical density is related to intensity and defined by:

$$OD = -log_{10}\left(\frac{I}{I_0}\right) \tag{4.1}$$

where I_0 and I are the readings for the unexposed (background) and irradiated film pieces, respectively, read from ImageJ [25]. The ODs were calculated with Equation 4.1 and converted to an absorbed dose with a calibration curve. The absorbed dose for one-second exposure was then estimated. Finally, the absorbed dose of each gel vial received was converted using specific irradiation times.

4.2.2 Small field measurement

Collimators with different sizes (3x3 mm^2, 5x5 mm^2, 10x10 mm^2) were attached to XenX's irradiation head to give steep dose gradients. Vials (diameter 2 cm, length 6 cm, volume 15 ml) were positioned at SSD = 34 cm and irradiated with 220 kV and 13 mA (Figure 4.2b). The exposure time was 240 s for each vial. Background subtraction was done using R_2 signals from an unirradiated vial and using R_2-dose-response relation from the same batch to convert to dose. In order to acquire R_2-dose-response relation, vials were irradiated with 1, 5, 10 and 15 Gy homogeneously and line fitting was performed, similarly to Dose response in photon beam.

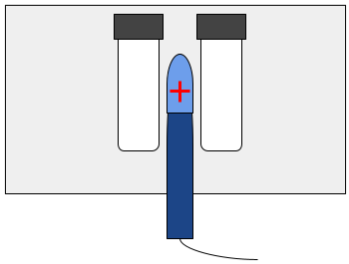

(a) Schematic figure of setup during irradiation in beam's eye view. Two gel vials are positioned on each side of an ionization chamber.

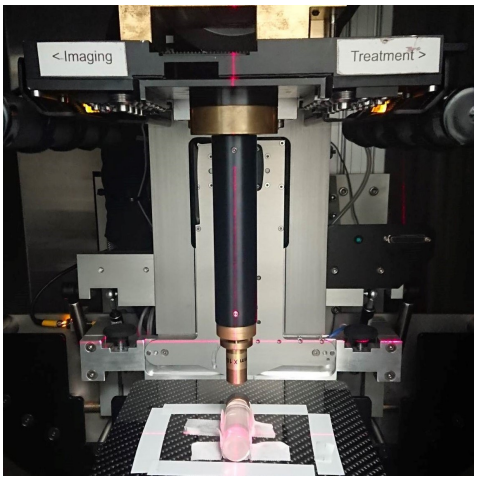

(b) Setup for the small field irradiation with an attached collimator on XenX's beam source.

Figure 4.2: Different setups with XenX irradiator for linearity test and small field measurement.

4.2.3 Intrabatch variation & Interbatch variation

Gel vials were used to examine intrabatch variation & inter-batch variation. One gel vial was irradiated at once at SSD = 34 cm with 220 kV XenX irradiator, the same setup as in Figure 4.2b. For interbatch variation, two separate batches of the same gel composition were produced (the same gel batches as in Dose response photon beam). The two gel batches with two gel vials per dose level for each batch were then scanned at the same time to reduce any potential influence of temperature on interbatch evaluation.
To investigate intrabatch variation, three dose levels (1, 5 and 15 Gy) were delivered and each was repeated eight times. Intrabatch was defined as the standard deviation of R_2 for each dose level/group.

4.2.4 Dose rate & Energy dependency

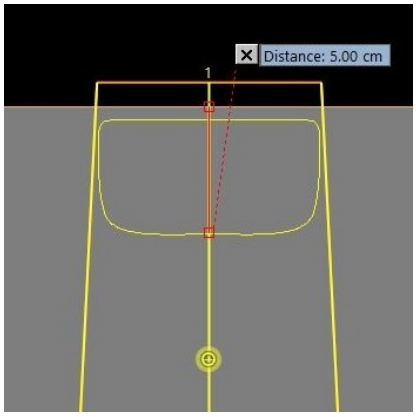

(a) Figure from Eclipse TPS, the yellow line indicates 100% isodose.

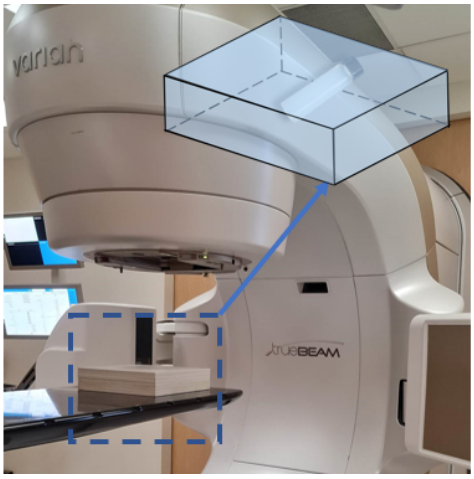

(b) Gel vial inside polystyrene slab on linear accelerator couch.

Figure 4.3: Irradiation setup with a linear accelerator.

Small vials were irradiated with a clinic linear accelerator at SSD of 90 cm using a 10x10 cm^2 field to investigate dose rate and energy dependence of the gel dosimeter (Figure 4.3b). The delivered doses were verified in Eclipse TPS so that 5 cm depth in water phantom would receive 100% planned doses (Figure 4.3a). The vials were placed inside a polystyrene slab (ρ= 1.005 g/cm^3), under 3 cm solid water plates (ρ=1.0 g/cm^3), irradiated with different energies (10 MV and 6 MV, both with dose rate 600 MU/min) and different dose rates (6 MV with dose rate 600 MU/min and 6 MV with 300 MU/min), one gel vial per dose level. Measured ROIs were taken at the centre of the gel vials (i.e. under 3 cm solid water plates, 1 cm polystyrene and approximately 1 cm NIPAM gel) to derive R_2 values for each measurement. The design of the polystyrene slab can be seen in Figure 4.4.
The number of MUs to deliver absorbed doses of 1, 2, 5, 10 and 15 Gy at 5 cm depth were calculated in the Eclipse TPS.

4.2.5 Dose response proton beam

The process of gel manufacturing and gel readout was carried out at SUS and LU in Lund, Sweden. Irradiation was carried out at Skandion Clinic, Uppsala, Sweden. Gel containers were small vials (2 cm diameter, 6 cm length, volume 15 ml) and larger vials (2 cm diameter, 13 cm length, volume 35 ml). To prevent photopolymerization, all vials were stored inside a refrigerator (set to 5 °C) inside a cardboard box for 4 hours before being transported from Lund to Uppsala. Following transportation, the gel was kept in cardboard at room temperature until irradiation.

4.2.5.1 Dose response at plateau region

Reference dose measurements for proton beam were performed using an ionization chamber (Roos Electron Chamber, plan parallel type, active region of 0.35 cm^3). A single layer field 10x10 cm^2 with spot size 3 mm, spot distance 2.5 mm, 1681 spots with 0.4 MU/spot, and energy 120 MeV was used. The monitor units were then rescaled to deliver dose levels of 0.5, 1, 2, 5, and 10 Gy with 498.07, 996.15. 1992.30, 4980.74, 9961.48 MU.
The gel vial was placed inside polystyrene slab (Figure 4.4 & 4.5). The rescaled MUs were delivered to gel vials (diameter 2 cm, length 6 cm, 15 ml) to deliver dose levels of 0.5, 1, 2, 5, and 10 Gy with two gel vials per dose level at 2 cm depth (1 cm solid water, 1 cm polystyrene). Gantry angle was set at 270° (Figure 4.5). Measured ROIs were acquired at approximately 3 cm depth (i.e 1 cm solid water, 1 cm polystyrene and approximately 1 cm in NIPAM gel), in the plateau region of the proton beam to derive R_2.

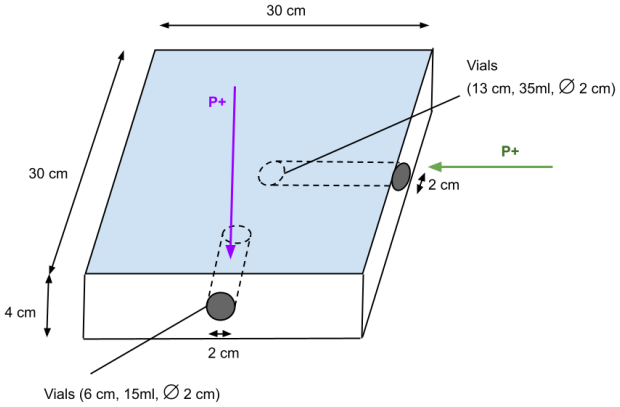

Figure 4.4: Design of polystyrene slab. Smaller vials (6 cm length, 15 ml, diameter 2 cm) were placed at 1 cm depth inside polystyrene slab. Irradiation was done perpendicular to the cylinder gel vial axis (purple arrow) for the measurement of dose response at the plateau of proton beam. For the depth dose measurement, bigger vials (13 cm, 35 ml, diameter 2 cm) were placed at 1 cm depth inside polystyrene slab and irradiation was performed along the axis of gel vials (green arrow).

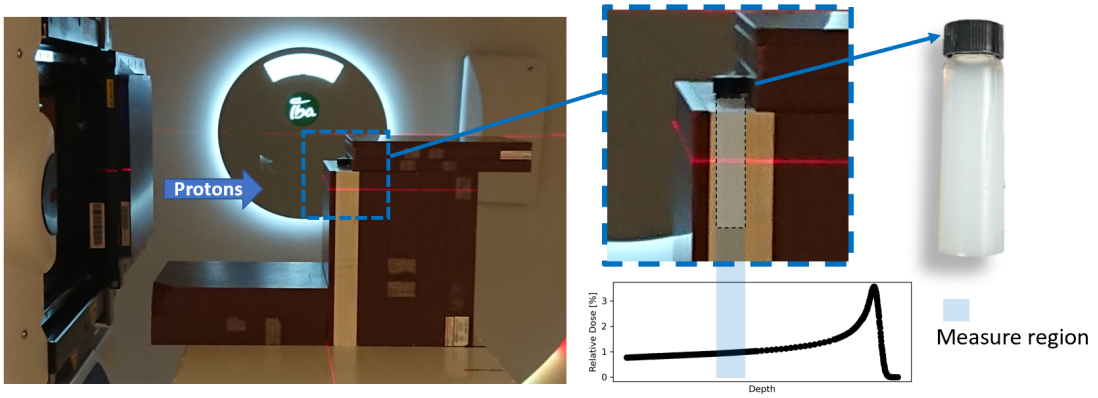

Figure 4.5: Setup for the proton dose-response measurement at plateau region. A gel vial (diameter 2 cm, length 6 cm, volume 15 ml) with lid on the outside was placed inside the polystyrene slab (white colour) and irradiated perpendicular to the axis of the cylinder gel vial. Solid water blocks (brown colour) were used to stabilize the slab and act as beam dump. One gel vial was irradiated at once with a single layer field 10x10 cm^2 of 120 MeV proton beam.

4.2.5.2 Depth dose measurement

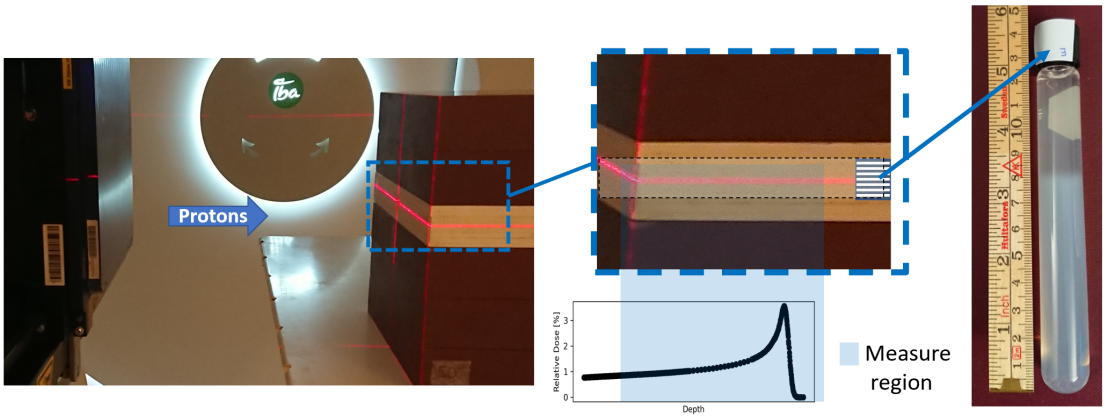

Figure 4.6: Setup for the depth dose measurement. The gel vial was placed inside polystyrene slab, and irradiated along the axis of gel vial, entrance dose was at the rounded end side of the vial. One gel vial was irradiated at once with a single layer field 10x10 cm^2 of 120 MeV proton.

Cylindrical vials (diameter 2 cm, length 13 cm, volume 30 ml) were irradiated so that the entrance dose would be at the rounded side of the vial for vials 1 (approximately dose at 2 cm depth was 0.5 Gy and 2 Gy at the Bragg peak) and 2 (approximately dose at 2 cm depth was 1 Gy and 4 Gy at the Bragg peak) (Figure 4.6). For vial 3 (approximately dose at 2 cm depth was 1 Gy and 4 Gy at Bragg peak), a 2 cm thick solid water block was placed before the beam penetrated the gel vial as beam attenuator to ensure the depth dose curve was positioned inside the glass vial. During irradiation, the lids for the vials were taken off for about 1.3 minutes due to

the size of the drill hole did not fit the lid. The monitor units delivered were 498.07, 996.15 and 996.15 MU for vials 1, 2, and 3 respectively. The choice of absorbed doses delivered was based on clinic relevance.
Measured curves were compared with a reference curve, a depth dose curve for a 120 MeV pristine proton beam measured with a large-area Bragg peak chamber (PTW-Freiburg Model 34070), diameter 8.16 cm, measured in water medium, corrected with Monte Carlo calculation.

4.3 Clinical application in 3D dose measurement: Multiple metastases HyperArc SRS photon treatment verification

In order to evaluate the NIPAM-gel dosimeter and assess its potential for clinical use, the dose distribution acquired with the gel dosimeter was compared to treatment planning system (TPS) for a multiple metastases HyperArc treatment.
The gel was transferred into one 1.2 litre flask/phantom (diameter 11 cm, length 23 cm) and twelve 15 ml gel vials (2 cm diameter, 6 cm length). The vials, together with the phantom, were set inside the fridge (5 °C) for 4 hours before computed tomography (CT) scanning. To prevent photopolymerization, phantom and vials were stored inside cardboard.

4.3.1 CT scanning

The gel phantom was fixated in a vacuum bag and positioned using lasers (Figure 4.7). The phantom was scanned with a clinical CT scanner (Siemens, SOMATOM Definition AS) using a scanning protocol for stereotactic brain treatment with a slice thickness of 1.0 mm. Vitamin-E capsules were placed on the surface of the gel phantom to facilitate image registration between CT and MR images. $CTDI_{VOI}$ for CT scanning was estimated directly on the CT scanner. After CT scanning, the gel was left in the dark one day prior to irradiation.

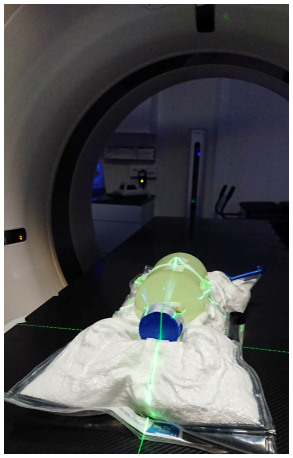

Figure 4.7: CT-scanning of gel phantom.

4.3.2 Dose planning

A clinical HyperArc plan was optimized for a patient with two intracranial metastases and was calculated with the anisotropic analytical algorithm (AAA) in TPS Eclipse (Version 15.6, Varian Medical System, Milpitas, CA). The prescribed dose was 30 Gy/3 fractions. The Gross Tumour Volumes (GTVs) were 3.0 cm^3 and 2.9 cm^3. The dose was normalized so that 100% corresponds to the dose covering 98% of the target volume (Planning Target Volume 1, PTV1) giving a peaked dose distribution with a max dose of 12.3 Gy (123 %).

Registration of the patient CT and the CT of the gel phantom was done manually with rigid registration in Eclipse TPS so that target volumes (PTVs) were positioned centrally in the gel phantom (Figure 4.8). The structures (PTVs and GTVs) of the clinical plan were transferred onto the gel phantom.

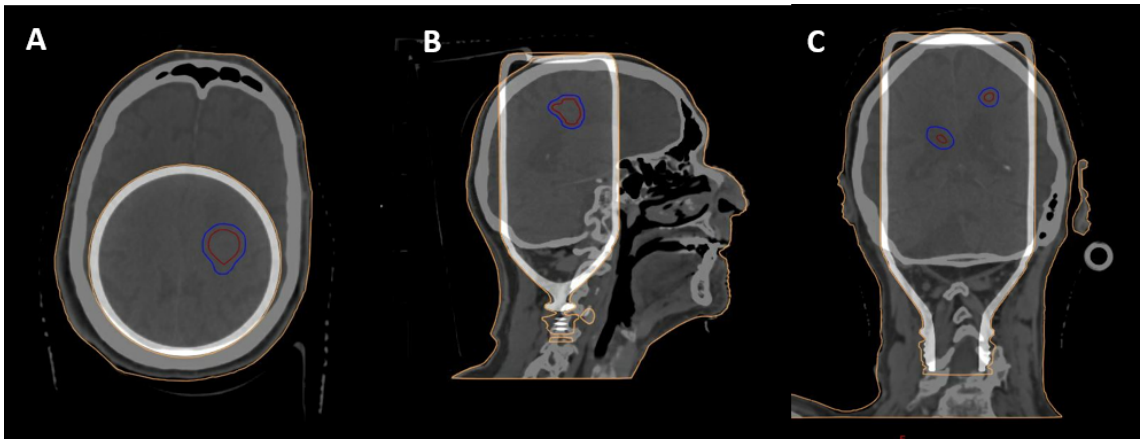

Figure 4.8: Registration of patient structure onto gel phantom in Eclipse TPS. PTVs are delineated with blue lines and GTVs are delineated with red lines, from left to right: A) Axial B) Sagittal C) Coronal.

The HyperArc plan was recalculated on the gel phantom using the same monitor units. The maximum dose to gel phantom was 13.3 Gy due to the difference in the anatomy of the patient and phantom. Dose distributions for the clinical plan and the recalculated plan on the gel phantom can be found in Figure 4.9. The plan was a four-partial-arc rotation, with the following monitor units for each arch: 759.1, 555.0, 622.3 and 555.8 MU (Figure 4.10b).

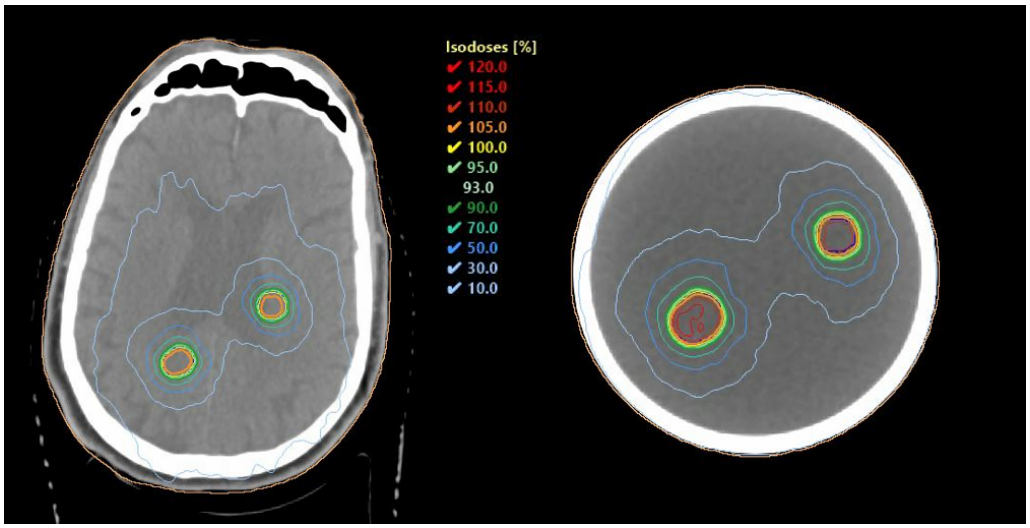

(a) Axial plane

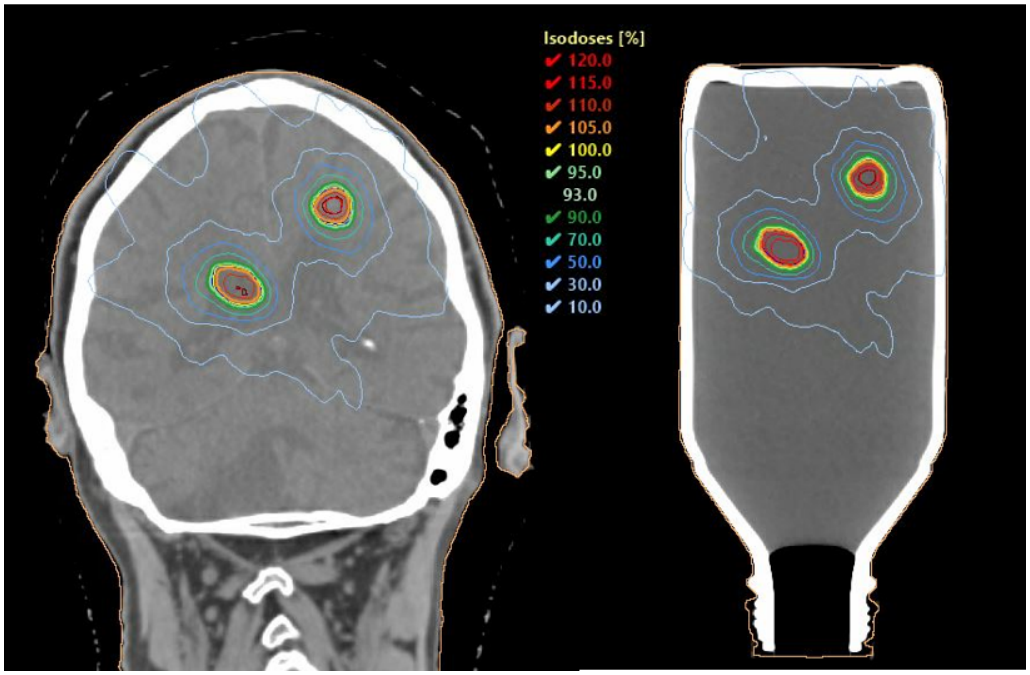

(b) Coronal plane

Figure 4.9: Clinical HyperArc plan with two intracranial metastases and recalculated dose plan for gel phantom. The figures are generated in Eclipse TPS.

4.3.3 Irradiation

The HyperArc plan was delivered to gel phantom (1.2 liters) using a clinical linear accelerator (Varian True Beam) with high-definition multi-collimator leaves (HD MLC) (0.25 cm wide in the isocenter and 0.5 cm wide outside the central region) (Figure 4.10a).

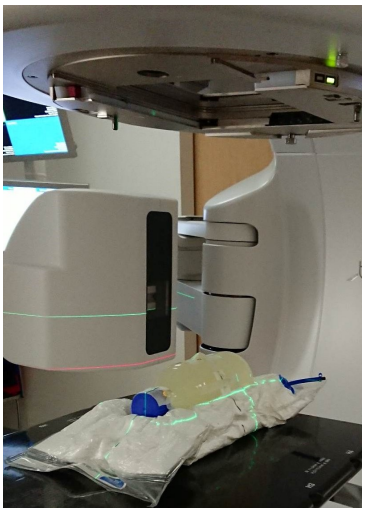

(a) Gel phantom was positioned on linear accelerators couch

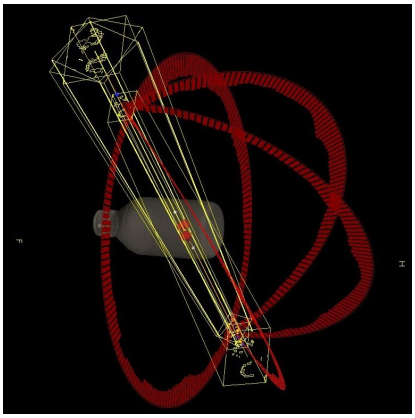

(b) Illustration of four partial-arc rotations. The couch was rotated in between arcs, the figure is generated in Eclipse TPS. Red lines show the movement of gantry rotation, yellow lines show the opening of the fields and red structures are the GTVs.

Figure 4.10: Gel phantom on linear accelerators couch and illustration of four partial-arc rotations of HyperArc treatment.

The flask was positioned with lasers according to markers drawn from CT scanning. A cone beam CT (CBCT) image was then taken with a clinical head protocol (100 kV, 150 mAs, half trajectory). $CTDI_{VOI}$ for the CBCT was estimated directly on the linear accelerator. The CBCT and CT-images were automatically matched in six degrees of freedom (lateral, longitudinal, vertical, pitch, rotation and roll). The couch was corrected in the lateral, longitudinal, vertical, pitch and rotation directions.
Small vials (diameter 2 cm, length 6 cm, 15 ml) were placed inside a polystyrene slab with a similar setup as in the Dose rate & Energy dependency test. The vials were irradiated with 6 MV photon at a dose rate 600 MU/min and dose interval 0-15 Gy to verify the linearity of R_2-dose response for the gel batch. A 10x10 cm^2 field was used, SSD was 90 cm and the gel was positioned at 5 cm depth in the phantom. The delivered doses were verified in Eclipse TPS so that 5 cm depth in water phantom would receive 100% planned doses. The specific MUs to deliver absorbed doses of 1, 2, 5, 10 and 15 Gy at 5 cm depth were calculated in TPS in a homogenous water phantom.

4.4 Magnetic Resonance Imaging (MRI) readout

A clinical MRI scanner (GE Signa Architect 3 T) together with an AIR^{TM}-flex coil (GE) and a spinal coil (GE) were used for scanning (Figure 4.11a). T_2 weighted

imaging was performed with a 16 multiple spin-echo pulse sequence (min TE 76 ms, max TE 1200 ms, echo spacing 75 ms, auto TR ranging from 6060 to 9647 ms, bandwidth 390.6 Hz/pixel, flip angle & Refocus 90°). The multi spin-echo sequence was modified by Emil Ljungberg (a postdoctoral student in Medical Radiation Physics, LU) with pulse programming. The gel dosimeters (vials and flask) were placed in the clinical MR-scanner room prior to scanning to stabilize and homogenise temperature. As mentioned before, exposure time to ambient light was minimized to the gel dosimeters in order to avoid the effect of photopolymerization. All MRI-scan sessions were performed at approximately one day post-irradiation. T_2-weighted images were reconstructed with AIR Recon DL, an AI-based image reconstruction method from GE. The setup of different scans is presented in Figure 4.11.

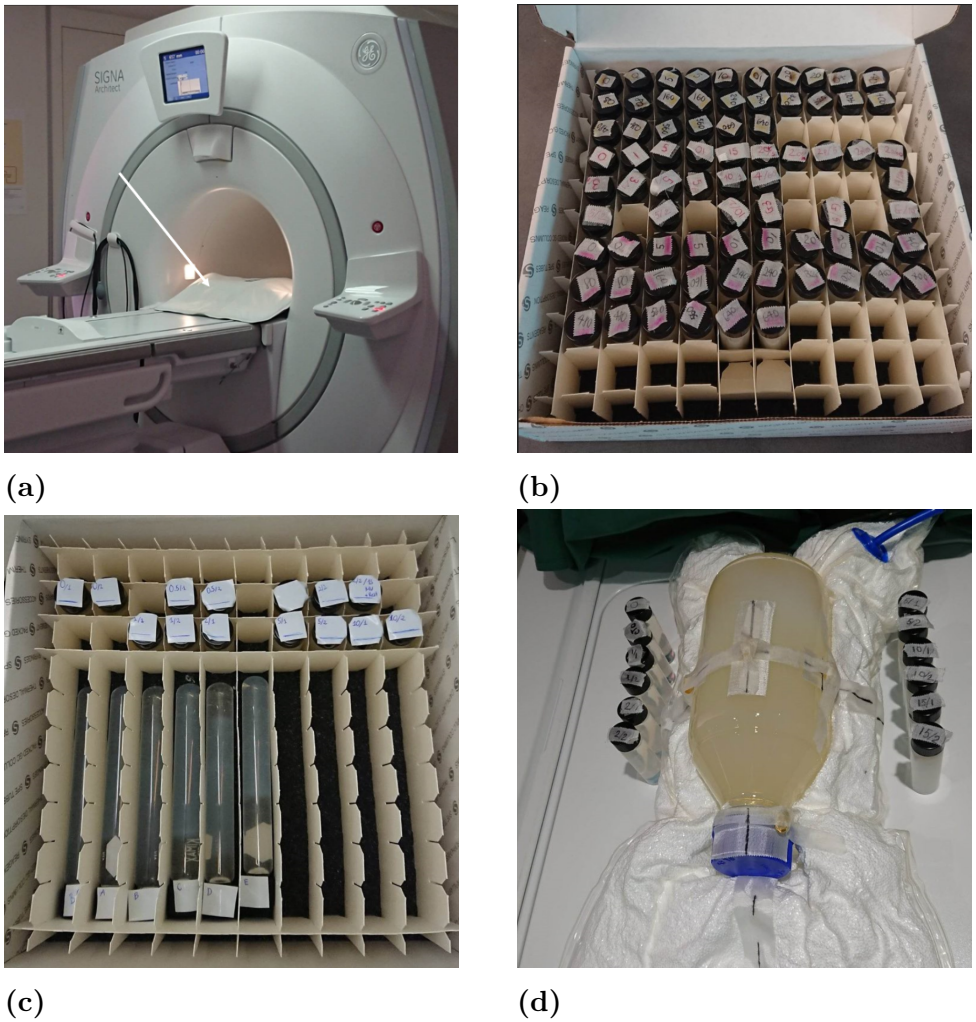

Figure 4.11: The setup of different MRI scans: a) Scanner GE Signa Architect and AIR^{TM}-flex coil (white arrow) and built-in spinal coil in the patient couch; b) A typical setup with small vials (volume 15 ml) inside a cardboard box; c) Setup image for scanning of vials irradiated with proton beam (both small, volume 15 ml, and bigger vials, volume 35 ml); d) Set up for scanning of gel phantom and small vials to confirm linearity. During scanning, AIR^{TM}-flex coil was positioned on top of a closed cardboard box, in a) and b), or gel phantom and small vials, in d).

4.4.1 Investigation of characteristics of the NIPAM gel dosimeter

4.4.1.1 Photon irradiation

The gel dosimeters (vials and flask) were placed in the clinical MR-scanner room one day prior to scanning. MRI scan parameters are listed in Table 4.2. Coronal scans were used for the analysis of Dose reponse photon beam, Intrabatch & Interbatch variation, Dose rate & Energy dependency; both coronal and axial scan was used for the analysis of small-field measurement (Table 4.2). A higher number of slices was collected to minimize the effect of possible artefacts. Data analysis was performed on one slice.

Table 4.2: MRI scan parameters to obtain dose distribution

Scan parameter	COR	AX
Voxel size [mm^3]	1.0x1.0x2.0	1.0x1.0x2.0
Slice spacing [mm]	0.6	0.6
FOV (Frequency x Phase)	256x256	256x256
Numer of excitation	2	2
Scan time [h]	2-3	2.5

4.4.1.2 Proton irradiation

Once the proton irradiation was completed, the gel was carefully placed inside a cardboard box and transported to SUS in Lund. To obtain the result for the dose response at the plateau for proton beam, small vials (15 ml) were scanned in the coronal direction, while the sagittal direction scan was performed to generate the depth dose curve for the larger vials (30 ml) (Figure 4.15b). The gel dosimeters were placed in cardboard during storage time and placed inside the MR-scanner room one hour prior to scanning. MRI scan parameters to obtain dose distribution are listed in Table 4.3. Although a higher number of slices was collected to minimize the effect of possible artefacts, one slice was chosen to perform analysis.

Table 4.3: MRI scan parameters to obtain dose distribution

Scan parameter	COR	SAG
Voxel size [mm^3]	1.0x1.0x2.0	1.0x1.0x5.0
Slice spacing [mm]	0.6	0.6
Matris size (Frequency x Phase)	256x256	256x256
Number of slices	26	31
Numer of excitation	3	1
Scan time [h]	2.5	2.5

Clinical application in 3D dose measurement: Multiple metastases HyperArc SRS photon treatment verification

The gel phantom and small gel vials were placed in the clinical MR-scanner room four hours prior to scanning. During scanning, the gel phantom and gel vials were positioned under the GE AIR^{TM} flex coil. The only time gel phantom and gel vials were exposed to light was during positioning with lasers for MR-scanning and CT-scanning. Scanning parameters are listed in Table 4.4.

Table 4.4: MRI scan parameters to obtain dose distribution

Scan parameter	COR
Voxel size [mm^3]	1.0x1.0x2.0
Slice spacing [mm]	0.0
Matris size (Frequency x Phase)	256x256
Number of slices	161
Numer of excitation	1
Scan time [h]	5.5

4.5 Data analysis

The image-processing program Hero version 2023.1.0 (Hero Imaging AB, Umeå, Sweden) was used to analyse the results. 16 T_2 weighted maps were acquired with multi-spin echo sequences. χ^2-minimization algorithm was applied by fitting intensities of equidistant consecutive images to Equation 3.4, excluding the first echo, to give T_2 value and then R_2 for every voxel. Due to the pronounced effect of the stimulated echoes causing the second echo signal to be higher than the first echo, the choice of excluding the first echo was made based on actual signals of 16 T_2-weighted maps to improve the fitting [26] (Figure 4.12).

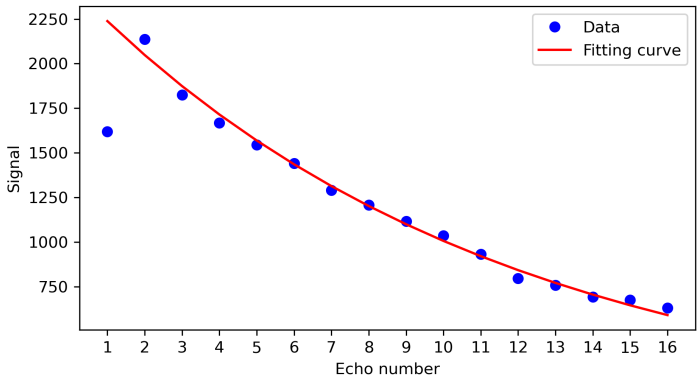

Figure 4.12: An example of signal/intensity curve for an ROI in 16 T_2-weighted maps with the actual scan parameters, used in this study (Table 4.2).

4.5.1 Investigation of characteristics of the NIPAM gel dosimeter

4.5.1.1 Photon irradiation

T_2-weighted maps were acquired with 16 spin echoes in a 2D coronal plane through the centre of the gel vial group. First, ROIs were drawn by creating binary masks with Otshu method. The ROIs were decreased in size with erode function to cover about 20% area of the vial (Figure 4.13).

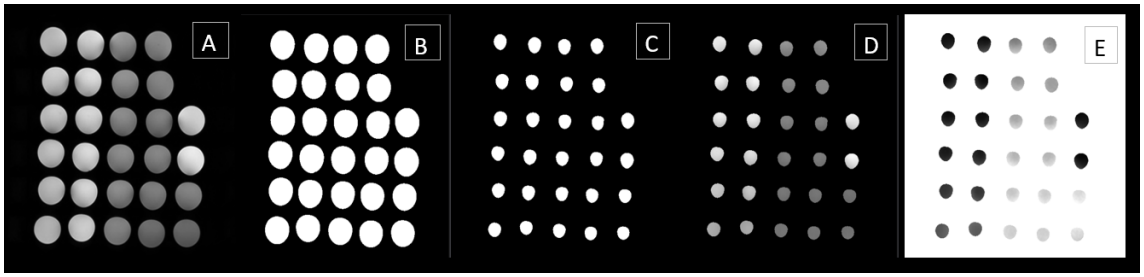

Figure 4.13: The process of acquiring R_2/T_2-maps in Hero for linearity test: A) A slice of T_2- weighted map of vials irradiated homogeneous, coronal plane. B) Binary masks. C) ROIs were created by eroding the binary masks D) T_2-maps acquired within eroded ROIs E) R_2-maps.

For the small field resolution test, R_2-maps in the axial plane were acquired (Figure 4.14). A dose profile was collected along the axis of the cylinder vial on R_2-maps to give a dose profile. Relative doses were background subtracted with an unirradiated vial, converted to dose using R_2-dose response relation and normalized to the central region value of the dose profile.
The dose profiles obtained from vials irradiated with different collimator sizes were compared with TPS (μ-RayStation, Raysearch), a software platform for planning and evaluation in small animal irradiation research. The gel vial was simulated using a cylinder with 2 cm in diameter and 1 mm thick glass surface. The density of the gel was approximated as water and the density for the glass was set to 2.33 g/cm^3. The dose distributions were acquired in TPS μ-RayStation using Monte Carlo simulation. The line profiles for each irradiation were collected along the axis of the cylinder, similar to dose profile acquired from gel vial. The full width at half-maximum (FWHM), i.e. the profile width at 50% the relative absorbed dose level for dose profiles obtained from the gel and μ-RayStation TPS were compared after interpolation.

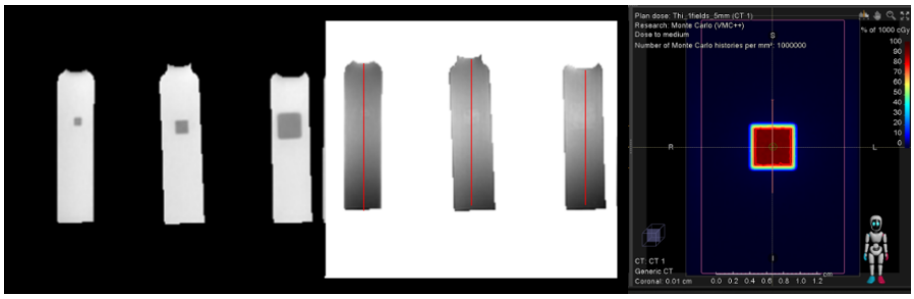

Figure 4.14: Small field measurement. From left to right: T_2-map, R_2-map, axial plane, for vials irradiated with different collimators (line profiles were drawn along the axis of cylinder vial, illustrated with red lines) and illustration of how line profile was extracted from μ-RayStation.

4.5.1.2 Proton irradiation

Analysis for dose response for proton beam at plateau region was similarly to the previous part with smaller vials (15 ml) (Figure 4.13).
Dose profiles parallel to the incident beam were extracted for each irradiation. Background subtraction was done with the distal region after the Bragg peak for each specific irradiation and normalization at 60 mm depth was done to obtain normalized depth dose curves for each vial. The measured curves were compared with the reference curve, both were normalized at 60 mm depth. The peak value (maximal value) was defined as the maximal value of the depth dose curve, i.e. the Bragg peak. The plateau value is defined at 60 mm depth to avoid uncertainty in the artefact region. Peak-to-plateau ratio (Peak/plateau) is defined as the quotient between these two values. The background subtraction and normalization method were based on previous work from Bäck et al. [27].

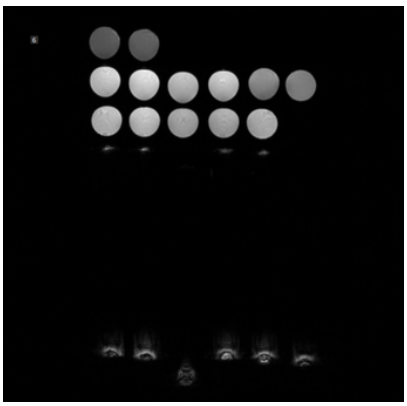

(a) One slice of T_2-weighted map at 16th echo, coronal plane to assess the dose response for proton beam at plateau region, the process of deriving R_2 is explained in Figure 4.13.

(b) One slice of T_2-weighted map at 16th echo, sagittal direction to obtain depth dose curve, artefact appeared at the rounded end of all the long vials which covered the first 3 cm of the vial.

Figure 4.15: One slice of T_2-weighted map, 16th echo, sagittal and coronal plane.

4.5.2 Clinical application in 3D dose measurement: Multiple metastases HyperArc photon treatment verification

The evaluation of linearity of the gel phantom using small vials was similarly to the previous part with smaller vials (15 ml) (Figure 4.13).
To obtain the dose distribution for the gel phantom, several steps were taken. First, CT and MR images were matched using rigid transformation with mutual information and point registration of Vitamin E markers, CT images were defined as fixed and MR images were defined as moving. Next, due to differences in spatial resolution between CT and MRI images (1x1x1 mm^3 and 1x1x2 mm^3 respectively), the dose distributions were linearly interpolated and resampled to 2x2x2 mm^3. Background subtraction was then performed using a volume which received a low dose in the flask, VOI_{bg}= 0.3 cm^3, and the dose distribution was normalized to a homogeneous dose region in PTV1, VOI_{norm}= 0.1 cm^3. The method for background subtraction and normalisation was based on previous work [6]. Finally, the dose distribution obtained from gel measurement was compared with the dose distribution obtained from Eclipse TPS by using global gamma criteria of 5%/5mm, 3%/3mm and 3%/2mm with thresholds corresponding to 90% of the prescribed dose (VOI_{90}) and 50% of the prescribed dose (VOI_{50}).

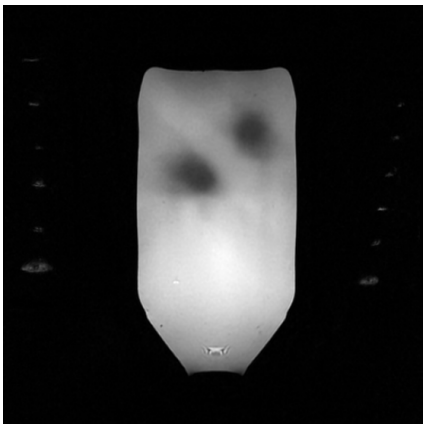

Figure 4.16: One slice of T_2-weighted map at 16th echo, coronal plane.

5
Results & Discussion

5.1 Establishment of gel dosimetry workflow

As part of this study, a workflow and protocol for the gel dosimetry methodology were optimized. There is currently no established protocol for how many hours the gel needs to be scanned after irradiation. Previous work suggested a scanning window of up to 72 hours [7]. For this study, MRI scanning was performed approximately 24 hours after irradiation, usually 28 hours, depending on the availability of the facilities.
The factors that affect the precision and accuracy of gel dosimetry can be found in each phase of the methodology: manufacturing, irradiation and imaging [5]. The manufacturing and irradiation steps were optimized with good practice. The manufacturing of the gel dosimeter was done in a careful and precise manner so that the concentration of chemical compounds stays the same for each gel batch. The dosimeters were placed inside MRI scanner room prior to scanning to homogenise temperature. The irradiation step was done so that positioning error was minimized by using lasers for alignment. The influencing factor for the imaging step is related to the T_2 measurement, which is affected by systematic errors during MRI scanning of the gel dosimeters. These errors include B0 and B1 fields nonuniformities, gradient nonuniformities, noise in the images and artefacts, which can affect the derived quantitative R_2 maps. For the study, to mitigate the problem with artefacts, GE AIR Recon DL was used to reconstruct images in order to enhance SNR and reduce artefacts such as Gibbs ringing (Appendix A.1). However, additional investigation is needed to determine the source of the susceptibility artefacts to prevent their effect in the future and shorten the scan time for the readout phase as only one slice was required for analysis of several tests (Figure 4.15b).

5.2 Investigation of characteristics of the NIPAM gel dosimeter

5.2.1 Dose response photon beam

Figure 5.1 illustrates the R_2 dose response over the interval 0-26 Gy for two batches.

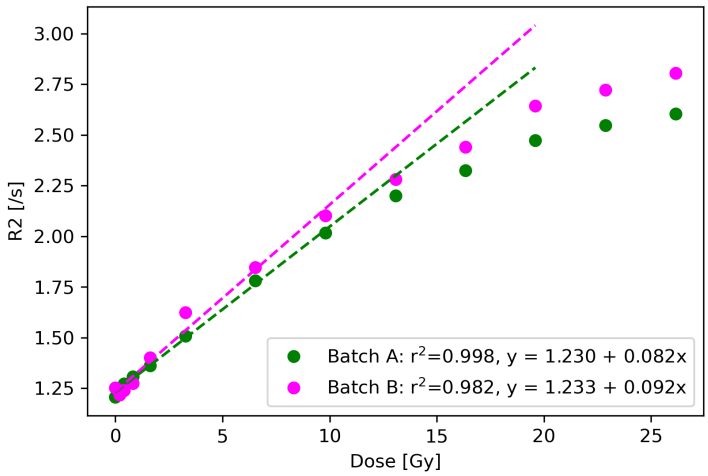

Figure 5.1: Dose response of NIPAM gel irradiated with 220 kV photon for two batches with the same gel composition. Fitting lines are generated for both batches over the interval 0-10 Gy.

Observing the scatter plot of two different batches, irradiated with 220 kV photon, an approximately linear R_2-dose response was observed for absorbed doses in the investigated interval with two batches, up to 10 Gy. However, the gel started to show non-linearity in high doses of approximately >10 Gy relative to the dose delivered (Figure 5.1). A previous study by Farajollahi et al. [28] reported an approximately linear dose-response in the dose range between 0 Gy to 25 Gy. This is not unexpected and is a known limitation of the gel with this dosimetry technique.
Observing the scatter plot in Figure 5.1, both the linear model and quadratic model may appear to fit the set of data well. r^2-analysis is difficult to tell whether a linear model is statistically better as it only shows the correlation between R_2-signal and absorbed dose ($r^2 \geq 0.98$ were found for the interval of 0-20 Gy for both batches for linear model). To determine whether the quadratic model gives a significantly better fit to the data, F-test (Chow test) was performed under the null hypothesis that the quadratic model is not significant better than the linear model. The results indicated that within the interval of 0-10 Gy, the quadratic model is not significant better than linear model for batch A ($p = 0.1$, $p>0.05$) and batch B ($p = 0.07$, $p>0.05$).

5.2.2 Small-field measurement

Comparison of the measured lateral dose profile from NIPAM-gel dosimeter and dose profiles obtained from μ-RayStation TPS are presented in Figure 5.2.

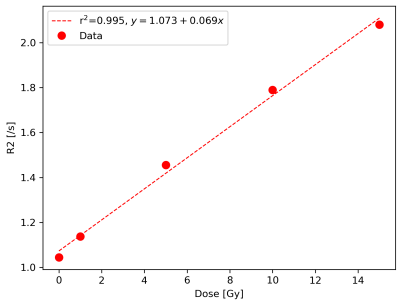

(a) R_2 dose response for the same batch

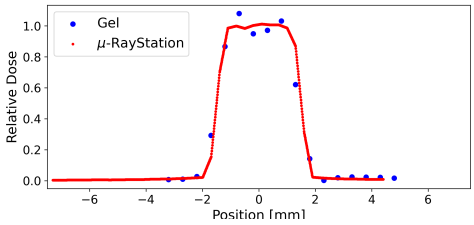

(b) 3x3 mm^2

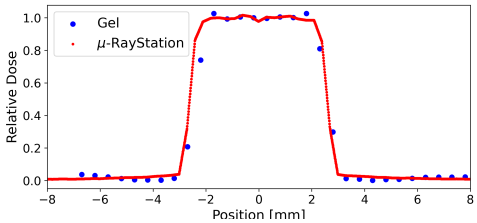

(c) 5x5 mm^2

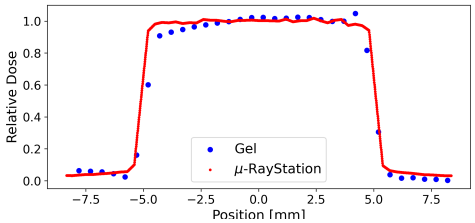

(d) 10x10 mm^2

Figure 5.2: Overlay of lateral dose profiles from the gel dosimeter and from μ-RayStation TPS with different collimator sizes and R_2 dose response for the same batch.

Table 5.1 presents the estimated FWHM for dose profiles obtained from the gel dosimeter and μ-RayStation TPS.

Table 5.1: FWHM-values for dose profiles obtained from gel and μ-RayStation TPS for different collimator sizes

Collimator size [mm^2]	μ-RayStation TPS [mm]	Gel [mm]	Δ [mm]
10x10	10.2	9.9	0.3
5x5	5.2	5.0	0.2
3x3	3.1	2.9	0.2

The results indicate good agreement between the FWHM from the gel dosimeter and the profile from the μ-RayStation TPS. However, the NIPAM gel dosimeter tends to slightly underestimate the dose profile relative to the TPS, with a maximum deviation of 0.3 mm, less than the in-plane resolution (Figure 5.2). One factor influencing the resolution of the gel dosimeter was the in-plane resolution of the MRI scanning used in this experiment, which was set at 1 mm x 1 mm. It is important to acknowledge that the gel dosimeter resolution is strongly coupled to the MRI in-plane resolution. Thus, achieving a higher resolution with the gel dosimeter would require a finer in-plane resolution during the MRI scanning process.
This observation highlights the importance of selecting an appropriate imaging technique to match the desired resolution requirements of the dosimetry system. In this case, improving the in-plane resolution of the MRI scans would likely result in a

higher resolution for the gel dosimeter and thus allow for a more accurate assessment of the dose profile.

5.2.3 Intrabatch & Interbatch variation

The result of response of NIPAM geldosimter for interbatch and intrabatch study is presented in Figure 5.3.

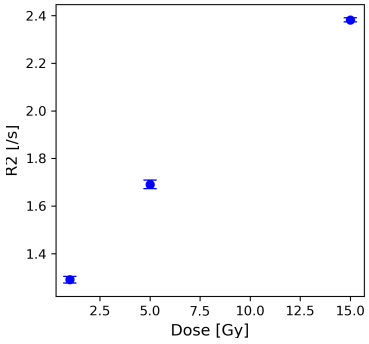

(a) Intrabatch result, batch C, consisted of 8 vials per dose level, the standard deviation for each dose level is included in the plot as bars.

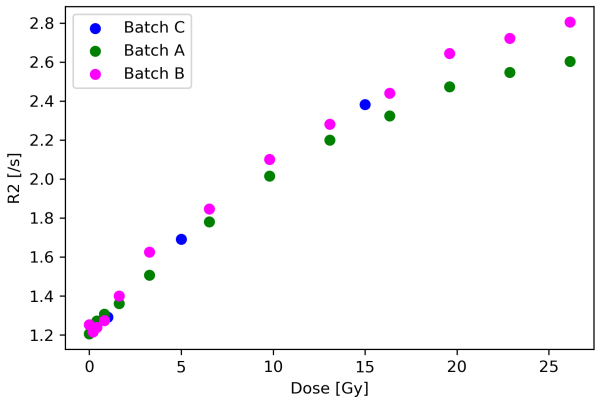

(b) Interbatch variation of three different batches A, B and C irradiated with 220 kV photon.

Figure 5.3: Result of response of NIPAM gel for inter batch and intrabatch study.

The intrabatch study resulted in the following average R_2 values and standard deviations: 2.4 ± 0.0087 s^{-1} for 15 Gy, 1.7 ± 0.018 s^{-1} for 5 Gy, and 1.3 ± 0.014 s^{-1} for 1 Gy (Figure 5.3a). The results show that relative standard deviation is within 1%. The maximal deviation of intrabatch was 3% within one dose level/group. In intrabatch experiments, the consistency of the response of the same batch of gel dosimeters to multiple absorbed doses was evaluated, providing information on the precision of the gel's response to radiation. The result of intra batch study indicates a good level of consistency within the same batch of gels.
In interbatch experiments, the consistency of the response of different batches of gel dosimeters to the same dose and same scanning was evaluated. The mean value of the interbatch variation was 4% for two batches scanned at the same time, with a maximum deviation of 7% at 26 Gy (Figure 5.3b). The plot in Figure 5.3b shows the comparison of different batches of gel dosimeters (batch A and B in the interval 0-16 Gy, scanned at the same time) together with batch C which was used for intrabatch test (dose interval 0-15 Gy, scanned in different days). Even though batch C was scanned on a different day, it demonstrated a similar dose-response to batch A and B, which were scanned on the same day, within a comparable dose range. One possible reason for this unexpected observation could be the relatively consistent temperature between the scanning days, and the stability of the gel compositions.

The result of intra and interbatch results are similar to the previous study from Farajollahi et al. which reported that the intrabatch reproducibility and interbatch reproducibility of NIPAM gel are 3% and 2%, respectively [28].

5.2.4 Dose rate & Energy dependency

The dose response data of NIPAM dosimeter irradiated with different energies (10 MV and 6 MV, both with dose rate 600 MU/min) and different dose rates (6 MV with dose rate 600 MU/min and 6 MV with 300 MU/min) in the absorbed dose interval 0-15 Gy are presented (Figure 5.4).

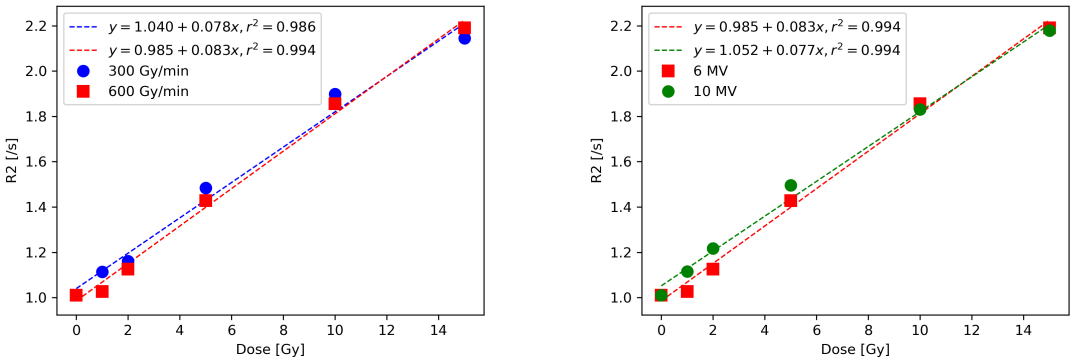

(a) Dose rates 600 MU/min and 300 MU/min, both with 6 MV photon energy.

(b) Different energies 10 MV and 6 MV, both with dose rate 600 MU/min.

Figure 5.4: Response of NIPAM dosimter irradiated with different energies and dose rates

Previous studies have reported conflicting results regarding the dose rate dependence of NIPAM gel dosimeters. Farajollahi et al. [28] investigated the dose rate dependence of NIPAM gel dosimeters to 6 MV photons and ^{60}Co and concluded that the dosimeter response is not affected by dose rate. In contrast, Waldenberg et al. [29] characterized the dose rate dependency of NIPAM gel dosimeters for dose rates of 100, 300, and 600 MU/min and found that the dose response is dependent on dose rate. The difference in these results could be attributed to variations in the experimental setup, dose interval, MRI scan parameter, methodology, sample size, and data analysis method. Further investigation is needed to confirm the dependency/independency of NIPAM gel to dose rate.
The average and maximum variation of R_2 between two dose rates were 4 and 8%, respectively, at 1 Gy. The results suggest that NIPAM gel dosimeters exhibit no dependence from dose rate at dose rates of 300 and 600 MU/min in the dose interval 0-15 Gy. However, further investigation is needed to ensure the reproducibility of the result.
Similarly, for the energy dependence study with 6 MV and 10 MV energy photons, the variation in R_2 value of different energies was at the largest 8% at 1 Gy and 2 Gy with an average deviation of 3%.

A previous study by Farajollahi et al. investigated the dose-response of NIPAM and found no dependence on energies of 1.25 MeV from ^{60}Co and 9 MV from a linear accelerator [28]. The results suggest that NIPAM gel dosimeters exhibit no energy dependence for 6 MV and 10 MV, which is in line with the previous study [28]. Further investigation is needed to ensure the reproducibility of the result.

5.2.5 Dose response proton beam

5.2.5.1 Dose response at plateau region

The result of dose response of the NIPAM gel dosimeter measured at the plateau region is presented in Figure 5.5. R_2 dose response, measured at plateau of proton depth dose curve shows an approximately linear response of NIPAM-based gel in the dose interval of 0-10 Gy, similar behaviour with 220 kV photon and MV photon after build-up region. Within the interval of 0-10 Gy, the p-value from F-test (Chow test) was found to be 0.23 (p>0.05), indicating that the quadratic model is not significant better than linear model. The results are also in line with prior works of gel dosimeters with proton beam [27, 30].

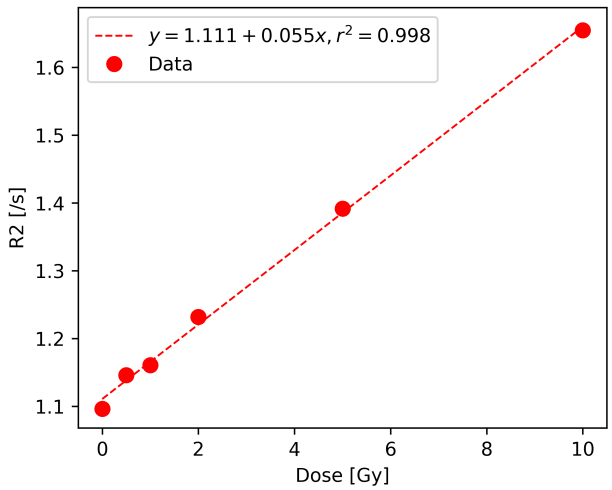

Figure 5.5: Dose response of NIPAM gel dosimeter to 120 MeV monoenergetic proton beam at the plateau region.

5.2.5.2 Depth dose curve measurement

Table 5.2 shows a comparison of reference/measured value of peak to plateau (peak/-plateau) ratio. The peak value is defined at the Bragg peak and the plateau is defined at 60 mm depth.

Table 5.2: Comparision of reference/measured value of peak to plateau ratio (peak/plateau), all the curves were normalized at 60 mm depth (plateau value). The reference curve was measured with pristine proton beam in water medium, measured 1 and 2 in NIPAM gel medium, measured 3 in 2 cm solid water and NIPAM gel medium.

	Peak/plateau
Reference	3.4
Vial 1	1.8
Vial 2	2.1
Vial 3	2.1

A comparison of measured curves in NIPAM gel medium and reference curves in water as a function of the depth of penetration for 120 MeV proton beam is presented in Figure 5.6.

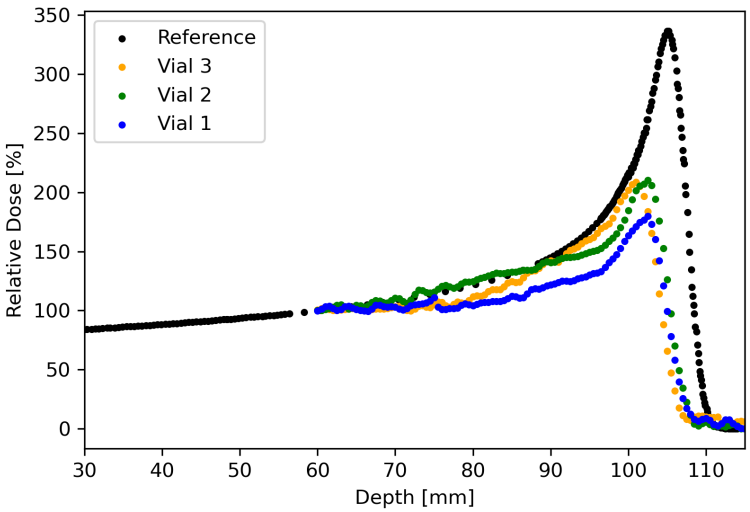

Figure 5.6: Relative depth-dose curves and reference, normalized at 60 mm depth. The reference curve was measured in water; the measured curves in NIPAM gel medium (vial 1, 2)/NIPAM gel medium and 2 cm solid water (vial 3).

Two additional vials were irradiated with entrance dose at the opening side (without lids), and the resulting images were excluded from analysis due to artefacts near the Bragg Peak, which made it difficult to determine the background level. Additionally, susceptibility artefacts at the beginning of the gel vials in MRI images made it challenging to determine the start of the gel medium. Due to this, the results from these vials are not reliable or accurate due to these technical difficulties and are thus not included in the result.
The amount of polymer produced in a polymer gel dosimeter is not solely determined by the incident radiation dose but is also affected by temperature. The background R_2 value, derived from an unirradiated gel vial, was higher (about 1.1 s^{-1}) for the smaller vial (15 ml) compared to the larger vial (30 ml) (about 0.8 s^{-1}), indicating

that the cooling rate (the time for the gel inside container to homogenise its temperature to the surrounding, most important during MRI scan) is also a factor that affects R_2. This finding is consistent with a previous study that suggests inaccuracies in polymer gel dosimetry may result from using small vials to do background subtraction to obtain dose distribution in larger gel containers [31]. Therefore, it is crucial to consider other variables in the procedure to improve the accuracy of polymer gel dosimetry.

The phenomenon of proton beam's signal at the Bragg peak when measuring with a gel dosimeter being lower than expected is usually referred to as the quenching effect. When the gel dosimeter is irradiated, water molecules in the gel are broken down into highly reactive free radicals and ions (such as $H\cdot$, $OH\cdot$, H_3O^+ ions and electrons) due to the radiolysis process. These free radicals and ions then react with the monomers in the gel, leading to the formation of polymer chains. For higher LET, the interaction sites are close together and the ion clusters overlap, which results a continuous ionisation around the track. At the higher LET region of the proton beam (i.e Bragg peak), radical recombination will increase with the decreased distance between the radicals. Thus, the amount of free radicals from water radiolysis decreases with increasing LET. Available radicals which are required for the polymerization decrease, consequently [32]. Thus, a lower signal at the Bragg peak region of measured curves in NIPAM dosimter was observed.

The peak-to-plateau ratio, obtained from NIPAM dosimeter, was lower than the reference peak-to-plateau dose ratio in water for the same proton energy (Table 5.2). The highest quenching effect was found for vial 1, approximately 0.5 Gy in absorbed dose at 2 cm depth, with approximately 45% lower value in peak-to-plateau ratio. Vials 2 and 3, approximately 1.0 Gy in absorbed dose at 2 cm depth, show approximately 40% lower value in peak-to-plateau ratio. The quenching effect was found to be more pronounced in vial 1 than compared to vials 2 and 3 (Figure 5.6). The results confirm that the quenching effect is related to LET variation. If the quenching effect were LET-independent, an empirical correction could be used to adjust the signal at each depth. However, further investigations are needed for the reproducibility of the result.

The quenching effect was observed in other gel dosimeters with protons in previous works [27] [30]. For instance, Bäck et al. [27] reported a 15% to 20% underestimation of the Bragg peak dose when using ferrous sulphate gels irradiated with a proton beam at 132 MeV. Similarly, Heufelder et al. [30] used BANG gel to investigate the depth dose curve and observed an underestimation of 25% to 30%. Both studies show a linear relationship between R_2 relaxation rates and dose, which holds in the case of constant LET, i.e when measured at the plateau region. However, large variation in LET led to the quenching of the Bragg peak region, a generic character in gel dosimeters.

A precise estimation of the measurement range for the experiment based on the acquired MRI images was challenging due to various factors. These include difficulties in determining the position of the gel medium due to artefacts together with minor misalignments of the vial during MRI scan and during irradiation inside the polystyrene slab. Consequently, accurately determining the true range in NIPAM gel and quantifying differences in the range between different measurements is a daunt-

ing task. Furthermore, in order to calculate the water equivalent thickness, data for relative stopping power for the exact energy and mass density for gel composition need to be available.
Other possible explanations of the difference between the measured and reference curve (in range and even small contribution in difference in peak to plateau ratio) were the differences in the setup. The reference curve was measured for a pristine proton beam of 120 MeV in a water medium, while the measured curve was obtained from a different medium (NIPAM gel or NIPAM gel and solid water). Additionally, the reference curve did not account for the presence of the gel glass container (approximately thickness of 1 mm), which was included in the measured curve. Achieving accurate results would require a correct water equivalent thickness of NIPAM gel which involves confirmation of mass density and the stopping power of the gel at the irradiated energy, as discussed, which is outside the scope of this thesis due to the limitation of time.
Additionally, the measurements in this work were done with a 120 MeV monoenergetic layer of proton beam. The study might have been more convincing if analysis for the linearity assessment and depth dose curve measurement of the proton beam included different energies and were performed over a wider dose range. However, due to the logistics of gel manufacturing, gel transporting, gel readout in this study (gel manufacturing and reading were done in Lund and irradiation was done in Uppsala), limited beam time the limited number of glass vials, the number of measurements were limited.

5.3 Clinical application in 3D dose measurement: Multiple metastases HyperArc photon treatment verification

R_2 dose response of the gel batch, evaluated with the small vials (15 ml), was found with r^2 =0.996 over the interval of 0-15 Gy for linear model (Figure 5.7). To further validate the linearity, F-test (Chow test) was conducted to compare the linear model with a quadratic model. The obtained p-value was 0.09. Therefore, the quadratic model is not significant better than the linear model over the interval of 0-15 Gy. The linearity of gel batch is confirmed over larger interval than 220 kV photon (Figure 5.1).

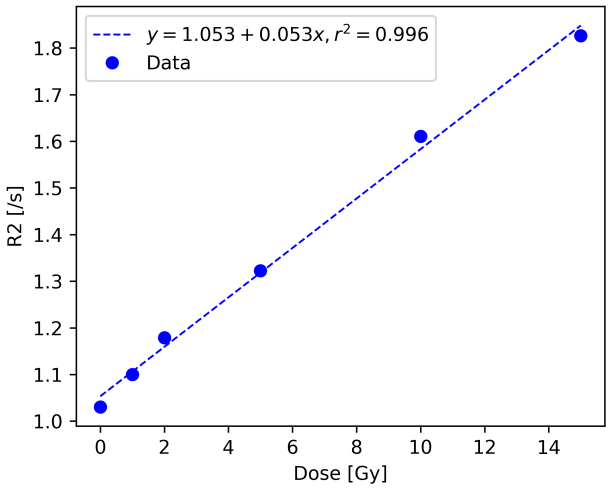

Figure 5.7: Dose response of NIPAM gel dosimeter to 6 MV photon beam to verify linearity for the gel phantom.

Illustration of 3D dose distribution of Eclipse TPS and gel phantom are presented (Figure 5.8).

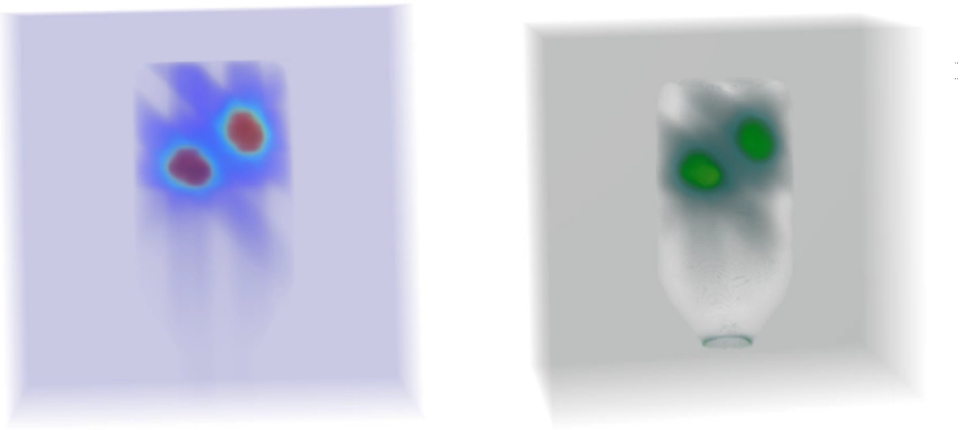

(a) Illustration of 3D dose distribution from TPS

(b) Illustration of 3D dose distribution from gel phantom

Figure 5.8: Illustrations of 3D dose distribution from TPS and gel phantom. The illustrations are generated from Hero.

One slice of the gamma map (3%/3mm) shows gamma failures observed along the surface of the gel container in Figure 5.9.

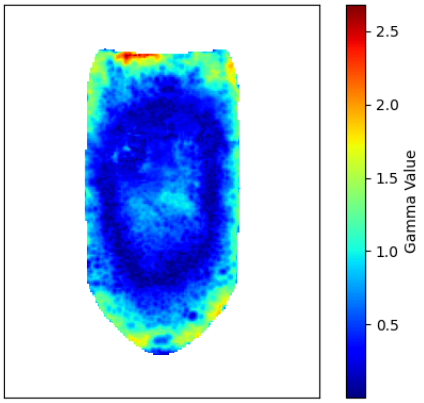

Figure 5.9: Gamma failures (3%/3mm) observed along the surface of the gel container in all directions, the plot shows one slice in coronal direction.

Line profiles through normalization region are presented in Figure 5.10.

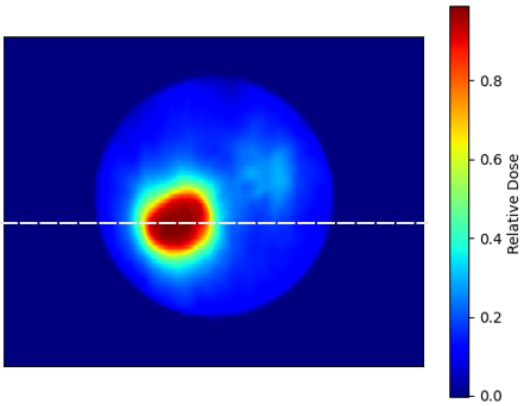

(a) Dose distribution from TPS to illustrate the location of normalization region and extracted line profile, axial plane.

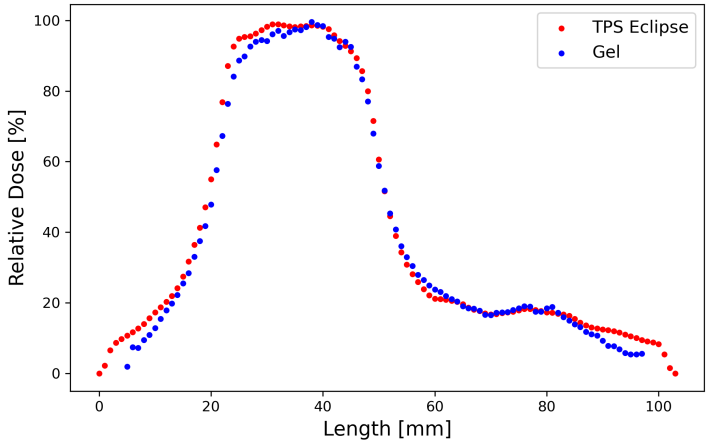

(b) Line profile through normalization region.

Figure 5.10: Line profile through normalization region, white dashed line in the dose distribution indicate the position of line profile.

Line profiles through high-dose regions of both targets are presented in Figure 5.11.

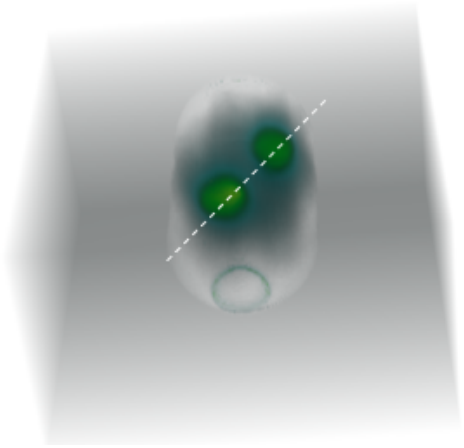

(a) Illustration of relative dose distribution from gel to extract line profile. The dose matrices were rotated to capture the high regions of both metastases. The figure is generated from Hero, white dashed line indicates the position of line profile.

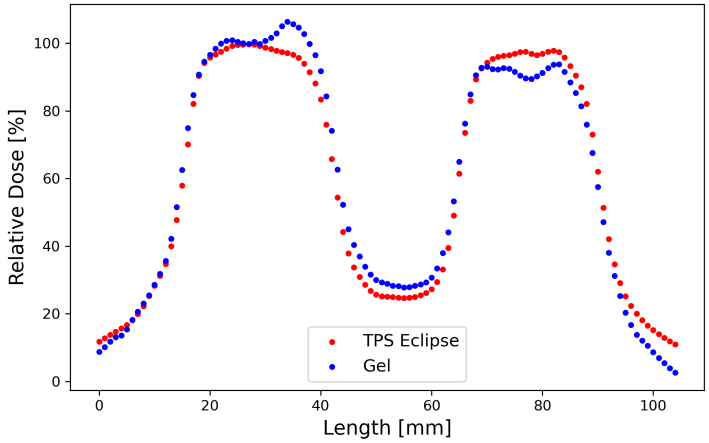

(b) Line profiles through high dose regions of both targets at the position of white dashed line.

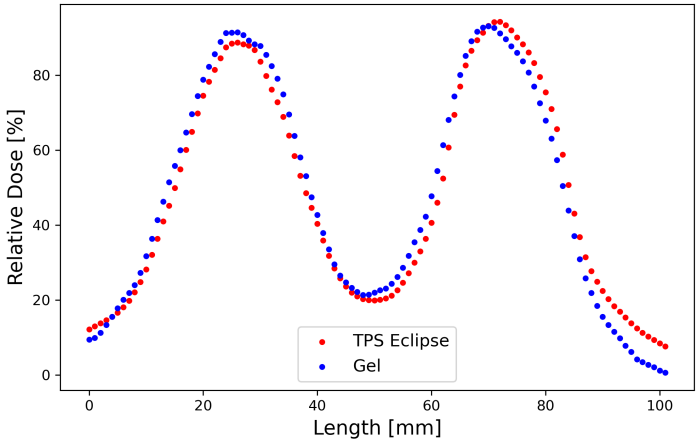

(c) Line profiles through high dose regions of both targets, 5 slices away from line profile in 5.11b.

Figure 5.11: Line profile through steep dose gradient regions of both metastases.

The pass rate for different gamma criteria in 90% dose volume (VOI_{90}) and 50 % dose volume (VOI_{50}), using dose distribution from Eclipse TPS as reference dose and dose distribution from NIPAM gel dosimeter as the measured dose is presented in Table 5.3.

Table 5.3: Pass rate for different gamma criteria in 90% dose volume (VOI_{90}) and 50 % dose volume (VOI_{50}).

Gamma criteria	5%/5mm	3%/3mm	3%/2mm
VOI_{90}	99.87	91.91	83.44
VOI_{50}	99.94	96.46	92.21

Slices with the high gamma fail clusters (gamma criteria 3%/3mm) for 50% of the dose for two PTVs are presented in Figure 5.12.

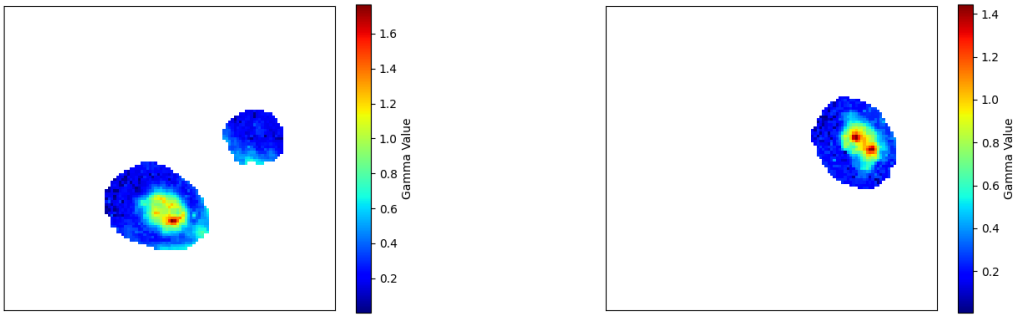

(a) Gamma map for VOI_{50} in PTV 2. **(b)** Gamma map for VOI_{50} in PTV 1.

Figure 5.12: One slice of gamma map for gamma criteria 3%/3mm in VOI_{50} for two targets, coronal plane.

$CTDI_{VOI}$ for the gel phantom was estimated at 28.8 mGy for acquiring a CT image. $CTDI_{VOI}$ from CBCT for positioning was measured at only 3.17 mGy. The effect of CT scanning on the change of R_2 was negligible when compared to the dosimetric quantity investigated in this study.
Gamma failures were observed along the surface of the gel container (Figure 5.9). The deviations were likely due to the inhomogeneity in the gel, caused by the faster cooling rate near the glass container wall after the gel solution was poured. The problem with the cooling rate coupled to R_2 was discussed before. Consequently, due to the unreliability of the gel dosimeter accuracy in these areas, it is advisable to avoid analyzing regions that are close to the surface of the gel container.
The choice of the background subtracted region and the normalized region was not an obvious choice. A HyperArc dose plane has a highly conformal dose distribution and a highly steep dose fall-off leaves the choice of normalized region which is required to be a homogenous dose region, being limited. Several normalization regions were chosen for analysis and the region which resulted in a higher gamma pass rate was chosen. Line profile through normalization region shows a relative homogeneous dose

region (Figure 5.10). Also, the region for the background subtracted was chosen in a region which received a relatively small dose. In previous work [6], the background subtracted value was acquired with an unirradiated flask with the same volume as the phantom, which might be a better approach.
A comparison of the pass rates between the NIPAM-gel dosimeter and TPS showed a high pass rate when using gamma criteria of 5%/5mm and 3%/3mm indicating good agreement between the two (Table 5.3). This suggests that the NIPAM gel dosimeter exhibits a certain level of reliability for 3D dose measurements, assuming TPS as the ground truth. To ensure the reproducibility of the results, it would have been beneficial to repeat the gel measurement and perform a comparison.
When stricter gamma criteria of 3%/2mm, commonly employed in clinical practice, were applied, the agreement between the gel and TPS decreased to 83.44% and 92.21% for VOI_{90} and VOI_{50}, respectively. The lower pass rate in the evaluation of VOI_{90} and VOI_{50} using the 3%/2mm gamma criteria could be attributed to the choice of background subtraction and normalized region together with inhomogeneity arose from the setting of gel or the absorbed dose might deviate from planned dose. The decrease in pass rate for V90% as compared to V50% indicates that there are larger deviations in the high dose area (Figure 5.11).
Upon observing the line profile through the normalization region, a good conciliation between the gel and TPS was shown (Figure 5.10a). However, clusters of gamma fails observed in the centre of the two metastases in Figure 5.12, can be explained by the response of the gel phantom in the high-dose region, as depicted in the line profile in Figure 5.11b. Notably, in a relatively high-dose region, the line profile located 5 slices away demonstrated good agreement (Figure 5.11c).

6
Conclusions

NIPAM gel dosimeter exhibited an approximately linear dose-response for various radiation qualities in the clinical relevant dose range, including 220 kV photons, 6 and 10 MV photons, and 120 MeV proton at the plateau region. The gel dosimeter demonstrated a high spatial resolution. Intrabatch variation shows good consistency with the maximal deviation of 3%. Interbatch deviation was found at with maximum of 7% at 26 Gy. Dose rate independency was found for dose rates of 600 MU/min and 300 MU/min within the 0-15 Gy dose range. Similarly, no energy dependency was observed for 6 MV and 10 MV within the same dose range.
When measuring the depth dose curve of the proton beam, the gel dosimeter exhibited a quenching effect of 40% to 45% in the Bragg peak due to higher linear energy transfer.
The result from verification of multiple brain metastases Hyper-Arc photon treatment showed pass rates of 99.94% and 99.87% (5%/5mm); 96.46% and 91.91% (3%/3mm) and 92.21% and 83.44% (3%/2mm) for VOI_{50} and VOI_{90}, respectively when compared to TPS.
The result of this study has improved the workflow for gel dosimetry, incorporating the use of new laboratory equipment, new MRI sequences during readout, and novel software for data analysis. Further, the results of this study enhance the understanding of NIPAM gel dosimeter characteristics and showed potential use for clinical applications in accurately assessing 3D dose distributions.

Acknowledgment

Above all, I would like to show my deepest gratitude to my supervisors Sofie Ceberg, Anneli Edvardsson, Crister Ceberg, Christian Jamtheim Gustafsson, Patrik Brynolfsson and Sven Bäck for their support and guidance throughout my work. Their insightful comments and different perspectives during meetings have been very valuable for the thesis. Working with them has been a great learning experience and an absolute pleasure.

I am grateful to the personnel from Skandion Clinic (Athanasia Christou, Alexandru Dasu and Malgorzata Liszka) who helped with the setup and irradiation for the proton experiment, especially Athanasia for her warm and lovely welcome. Special thanks to Emil Ljungberg, who modified the T_2 sequence for MRI. Thank you Elise Konradsson, who assisted with the finding of polystyrene slab and film irradiation. I would also like to acknowledge the contribution of engineer Lars Andersson-Ljus, who helped with the polystyrene slab for the experiment setup. Further, I would show appreciation to Victor Pham and Elinore Wieslander created and checked the HyperArc plan and Malin Kügele who helped to irradiate the Gelis phantom.
I would also want to thank the MRI and CT personnel at Skåne University Hospital for their time.

Thank you, Vivika, for being so supportive during these five years.
And to my classmates, thank you for being so kind to me during our studies.
Lastly, I want to express my deepest appreciation to my beloved family. Filip, thank you for your unconditional love and patience, and Tia, you are my endless source of joy.

Sincerely,
Thi (Lund, May 2023).

Bibliography

[1] Bray F, Laversanne M, Weiderpass E, Soerjomataram I. The ever-increasing importance of cancer as a leading cause of premature death worldwide. Cancer. 2021;127(16):3029-30. Available from: https://onlinelibrary.wiley.com/doi/abs/10.1002/cncr.33587.

[2] Baskar R, Lee KA, Yeo R, Yeoh KW. Cancer and Radiation Therapy: Current Advances and Future Directions. Int J Med Sci. 2012 Feb;9(3):193-9. Available from: https://www.ncbi.nlm.nih.gov/pmc/articles/PMC3298009/.

[3] Bedford JL, Lee YK, Wai P, South CP, Warrington AP. Evaluation of the Delta ^{4} phantom for IMRT and VMAT verification. Phys Med Biol. 2009 May;54(9):N167-76. Available from: https://iopscience.iop.org/article/10.1088/0031-9155/54/9/N04.

[4] Oldham M, Siewerdsen JH, Kumar S, Wong J, Jaffray DA. Optical-CT Gel-Dosimetry I: Basic Investigations. Med Phys. 2003 Apr;30(4):623-34. Available from: https://www.ncbi.nlm.nih.gov/pmc/articles/PMC1616153/.

[5] Baldock C, De Deene Y, Doran S, Ibbott G, Jirasek A, Lepage M, et al. Topical Review: Polymer gel dosimetry. Phys Med Biol. 2010 Feb;55(5):R1-R63. Available from: https://www.ncbi.nlm.nih.gov/pmc/articles/PMC3031873/.

[6] Ceberg S, Gagne I, Gustafsson H, Scherman JB, Korreman SS, Kjær-Kristoffersen F, et al. RapidArc treatment verification in 3D using polymer gel dosimetry and Monte Carlo simulation. Phys Med Biol. 2010 Sep;55(17):4885-98. Available from: https://iopscience.iop.org/article/10.1088/0031-9155/55/17/001.

[7] Kudrevicius L, Jaselske E, Adliene D, Rudzianskas V, Radziunas A, Tamasauskas A. Application of 3D Gel Dosimetry as a Quality Assurance Tool in Functional Leksell Gamma Knife Radiosurgery. Gels. 2022 Jan;8(2):69. Available from: https://www.ncbi.nlm.nih.gov/pmc/articles/PMC8871505/.

[8] Teoh M, Clark CH, Wood K, Whitaker S, Nisbet A. Volumetric modulated arc therapy: a review of current literature and clinical use in practice. Br J Radiol. 2011 Nov;84(1007):967-96. Available from: https://www.ncbi.nlm.nih.gov/pmc/articles/PMC3473700/.

[9] Soliman H, Das S, Larson DA, Sahgal A. Stereotactic radiosurgery (SRS) in the modern management of patients with brain metastases. Oncotarget. 2016 Feb;7(11):12318-30. Available from: https://www.ncbi.nlm.nih.gov/pmc/articles/PMC4914287/.

[10] Solberg TD, Balter JM, Benedict SH, Fraass BA, Kavanagh B, Miyamoto C, et al. Quality and safety considerations in stereotactic radiosurgery and stereotactic body radiation therapy: Executive summary. Pract Radiat On-

col. 2012 Jan;2(1):2-9. Available from: https://www.ncbi.nlm.nih.gov/pmc/articles/PMC3808746/.

[11] Albino LD, Khoury HJ, Roesler EH. Comparison Between Hyperarc and Conventional VMAT for Single and Multiple Brain Tumors Treated by Stereotactic Radiosurgery. International Journal of Radiation Oncology, Biology, Physics. 2020 Nov;108(3):e315. Publisher: Elsevier. Available from: https://www.redjournal.org/article/S0360-3016(20)32171-4/fulltext.

[12] Ohira S, Ueda Y, Akino Y, Hashimoto M, Masaoka A, Hirata T, et al. HyperArc VMAT planning for single and multiple brain metastases stereotactic radiosurgery: a new treatment planning approach. Radiat Oncol. 2018 Jan;13:13. Available from: https://www.ncbi.nlm.nih.gov/pmc/articles/PMC5789615/.

[13] Jette D, Chen W. Creating a spread-out Bragg peak in proton beams. Phys Med Biol. 2011 Jun;56(11):N131-8.

[14] Eric J Hall, Amato J Giaccia. Radiobiology for the Radiologist. 7th ed.; 2012.

[15] Cianchetti M. Sinonasal Malignancies and Charged Particle Radiation Treatment: A Systematic Literature Review. International journal of otolaryngology. 2012 May;2012:325891.

[16] Frese MC, Wilkens JJ, Huber PE, Jensen AD, Oelfke U, Taheri-Kadkhoda Z. Application of Constant vs. Variable Relative Biological Effectiveness in Treatment Planning of Intensity-Modulated Proton Therapy. International Journal of Radiation Oncology*Biology*Physics. 2011 Jan;79(1):80-8. Available from: https://www.sciencedirect.com/science/article/pii/S0360301609034130.

[17] McAuley KB, Nasr AT. Fundamentals of gel dosimeters. J Phys: Conf Ser. 2013 Jun;444:012001. Available from: https://iopscience.iop.org/article/10.1088/1742-6596/444/1/012001.

[18] Macchione MA, Lechón Páez S, Strumia MC, Valente M, Mattea F. Chemical Overview of Gel Dosimetry Systems: A Comprehensive Review. Gels. 2022 Oct;8(10):663. Number: 10 Publisher: Multidisciplinary Digital Publishing Institute. Available from: https://www.mdpi.com/2310-2861/8/10/663.

[19] Ceberg S, Lepage M, Bäck S, Gustafsson H, Ceberg C. Modelling the dynamic dose response of an nMAG polymer gel dosimeter. Phys Med Biol. 2012 Aug;57(15):4845-53. Available from: https://iopscience.iop.org/article/10.1088/0031-9155/57/15/4845.

[20] Pai A, Shetty R, Chowdhury YS. Magnetic Resonance Imaging Physics. In: StatPearls. Treasure Island (FL): StatPearls Publishing; 2022. Available from: http://www.ncbi.nlm.nih.gov/books/NBK564320/.

[21] Lepage M, Jayasakera PM. Dose resolution optimization of polymer gel dosimeters using different monomers. Phys Med Biol. 2001 Oct;46(10):2665. Available from: https://iopscience.iop.org/article/10.1088/0031-9155/46/10/310.

[22] De Deene Y, Baldock C. Optimization of multiple spin-echo sequences for 3D polymer gel dosimetry. Phys Med Biol. 2002 Sep;47(17):3117-41.

[23] Van Dyk J, Barnett RB, Cygler JE, Shragge PC. Commissioning and quality assurance of treatment planning computers. Int J Radiat Oncol Biol Phys. 1993 May;26(2):261-73.

[24] Low DA, Harms WB, Mutic S, Purdy JA. A technique for the quantitative evaluation of dose distributions. Medical Physics. 1998;25(5):656-61. Available from: https://onlinelibrary.wiley.com/doi/abs/10.1118/1.598248.

[25] Marroquin EYL, Herrera González JA, Camacho López MA, Barajas JEV, García-Garduño OA. Evaluation of the uncertainty in an EBT3 film dosimetry system utilizing net optical density. J Appl Clin Med Phys. 2016 Sep;17(5):466-81. Available from: https://www.ncbi.nlm.nih.gov/pmc/articles/PMC5874103/.

[26] Ben-Eliezer N, Sodickson DK, Block TK. Rapid and Accurate T2 Mapping from Multi Spin Echo Data Using Bloch-Simulation-Based Reconstruction. Magn Reson Med. 2015 Feb;73(2):809-17. Available from: https://www.ncbi.nlm.nih.gov/pmc/articles/PMC4169365/.

[27] Bäck S, Medin J, Magnusson P, Olsson P, Grusell E, Olsson LE. Ferrous sulphate gel dosimetry and MRI for proton beam dose measurements. Phys Med Biol. 1999 Aug;44(8):1983-96. Available from: https://iopscience.iop.org/article/10.1088/0031-9155/44/8/310.

[28] Farajollahi AR, Pak F, Horsfield M, Myabi Z. The basic radiation properties of the N-isopropylacrylamide based polymer gel dosimeter. Int J Radiat Res. 2014;12(4). Available from: http://ijrr.com/article-1-1354-en.html.

[29] Waldenberg C, Hauer AK, Gustafsson C, Ceberg S. Dose integration and dose rate characteristics of a NiPAM polymer gel MRI dosimeter system. J Phys: Conf Ser. 2017 May;847(1):012063. Publisher: IOP Publishing. Available from: https://dx.doi.org/10.1088/1742-6596/847/1/012063.

[30] Heufelder J, Stiefel S, Pfaender M, Lüdemann L, Grebe G, Heese J. Use of BANG polymer gel for dose measurements in a 68 MeV proton beam. Med Phys. 2003 Jun;30(6):1235-40. Available from: https://aapm.onlinelibrary.wiley.com/doi/abs/10.1118/1.1575557.

[31] Dumas EM, Leclerc G, Lepage M. Effect of container size on the accuracy of polymer gel dosimetry. J Phys: Conf Ser. 2006 Dec;56(1):239. Available from: https://dx.doi.org/10.1088/1742-6596/56/1/038.

[32] Gustavsson H, Bäck S, Medin J, Grusell E, Olsson LE. Linear energy transfer dependence of a normoxic polymer gel dosimeter investigated using proton beam absorbed dose measurements. Phys Med Biol. 2004 Sep;49(17):3847-55. Available from: https://iopscience.iop.org/article/10.1088/0031-9155/49/17/002.

A

Appendix

A.1 GE AIR Recon DL image

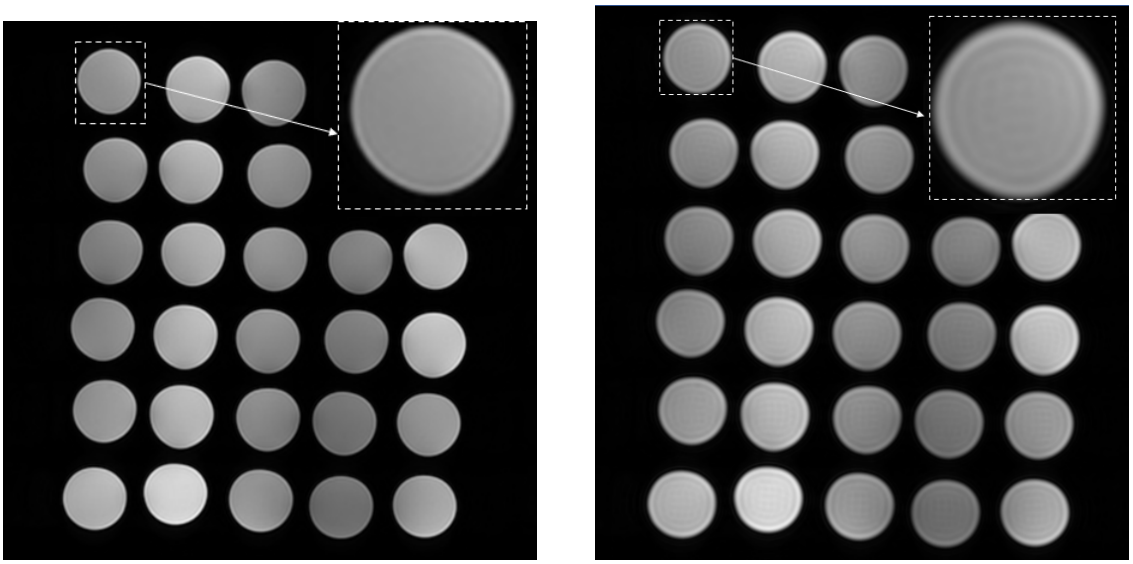

(a) GE AIR Recon DL T_2 map. **(b)** Original T_2 map.

Figure A.1: Comparision of T_2 map with GE AIR Recon DL reconstructed shows enhanced SNR and artefact reduction.